UNIVERSITY OF WEST BOHEMIA IN PILSEN
Faculty of mechanical engineering

Study programme: B2301 Mechanical Engineering
Field of study: Design of Power Machines and Equipment

DIPLOMA THESIS

Large eddy simulation of a turbulent flow
around a low pressure turbine blade

Author: **Bc. Lukáš HURDA**
Supervisors: **Ing. Roman Gášpár**
Prof. Laurent BRICTEUX
Consultants: **Ir. Rémy Nigro,**
Ir. Stéphanie Zéoli,
Ir. Marie Cordier

Academic year 2015/2016

ZÁPADOČESKÁ UNIVERZITA V PLZNI
Fakulta strojní
Akademický rok: **2015/2016**

ZADÁNÍ DIPLOMOVÉ PRÁCE

(PROJEKTU, UMĚLECKÉHO DÍLA, UMĚLECKÉHO VÝKONU)

Jméno a příjmení:	**Bc. Lukáš HURDA**
Osobní číslo:	**S14N0042P**
Studijní program:	**N2301 Strojní inženýrství**
Studijní obor:	**Stavba energetických strojů a zařízení**
Název tématu:	**Large eddy simulation of turbulent flow around a low pressure gas turbine blade**
Zadávající katedra:	**Katedra energetických strojů a zařízení**

Zásady pro vypracování:

1. Literature review
2. Case setup
3. Grid generation
4. Preliminary computations
5. Production runs
6. Result analysis
7. Writing report

Rozsah grafických prací: **2 - 5 výkresů formátu A2**

Rozsah kvalifikační práce: **50 - 70 stran**

Forma zpracování diplomové práce: **tištěná/elektronická**

Jazyk zpracování diplomové práce: **Angličtina**

Seznam odborné literatury:

- **Ferziger Joel H. a Perič Milovan: Computational methods for fluid dynamics. 3rd rev. ed. Berlin: Springer-Verlag, 2002, xiv, 423 s., ISBN 3540420746**
- **Steiger Rory Douglas, 2002: The Effects of Wakes on Separating Boundary Layers in Low Pressure Turbines, Cambridge, United Kingdom, PhD thesis, Cambridge University Engineering Department, Supervisor Prof. H. Hodson**
- **Dixon S. L. a Hall C. A.: Fluid mechanics and thermodynamics of turbomachinery, 6th ed. Burlington: Butterworth-Heinemann, 2010, 459 s., ISBN 978-1-85617-793-1**
- **Anderson J. D.: Computational fluid dynamics: The basics with applications, New York: McGraw-Hill, 1995, 547 s., ISBN 0-07-001685-2**
- **Moustapha H.: Axial and radial turbines, White River Junction, Vt: Concepts NREC, 2003, ISBN 9780933283121**

Vedoucí diplomové práce: **Ing. Roman Gášpár**
Katedra energetických strojů a zařízení
Prof. Laurent Bricteux
University of Mons

Konzultant diplomové práce: **Ir. Marie Cordier**
University of Mons

Ostatní konzultanti: **Ir. Rémy Nigro**
University of Mons
Ir. Stéphanie Zéoli
University of Mons

Datum zadání diplomové práce: **2. listopadu 2015**

Termín odevzdání diplomové práce: **20. května 2016**

Doc. Ing. Milan Edl, Ph.D.
děkan

L.S.

Západočeská univerzita v Plzni
Fakulta strojní

Ing. Zdeněk Jůza, Ph.D., MBA
vedoucí katedry

V Plzni dne 30. října 2015

SUMMARY OF DIPLOMA SHEET

AUTHOR	**Surname** Hurda	**Name** Lukáš	
FIELD OF STUDY	2302T013 “Desing of Power Machines and Equipment“		
SUPERVISOR	**Surname (Inclusive of Degrees)** Ing. Gášpár	**Name** Roman	
INSTITUTION	ZČU - FST - KKE		
TYPE OF WORK	**DIPLOMA**	~~**BACHELOR**~~	**Delete when not applicable**
TITLE OF THE WORK	Large eddy simulation of a turbulent flow around a low pressure turbine blade		

FACULTY	Mechanical Engineering		**DEPARTMENT**	Power System Engineering		**SUBMITTED IN**	2016

NUMBER OF PAGES (A4 and eq. A4)

TOTALLY	65		**TEXT PART**	65		**GRAPHICAL PART**	0

BRIEF DESCRIPTION **TOPIC, GOAL, RESULTS AND CONTRIBUTIONS**	This thesis dissert on assesing the solvers for fluid dynamics simulation of an incompressible turbulent flow in a low pressure turbine cascade using the Large Eddy Simulation. Simulations are carried out using high performance massively parallel computing facilities. The flow characteristics and solver runtime analysis are the key tools of the analysis.
KEY WORDS	LES, jet engine, gas turbine, CFD, OpenFOAM, YALES2, massively parallel computing, numerical simulation

ANOTAČNÍ LIST DIPLOMOVÉ PRÁCE

AUTOR	**Příjmení** Hurda	**Jméno** Lukáš	
STUDIJNÍ OBOR	2302T013 „Stavba energetických strojů a zařízení“		
VEDOUCÍ PRÁCE	**Příjmení (včetně titulů)** Ing. Gášpár	**Jméno** Roman	
PRACOVIŠTĚ	ZČU - FST – KKS		
DRUH PRÁCE	**DIPLOMOVÁ**	~~**BAKALÁŘSKÁ**~~	**Nehodící se škrtněte**
NÁZEV PRÁCE	Numerická simulace turbulentního proudění v nízkotlaké turbínové lopatkové kaskádě pomocí metody LES		

FAKULTA	strojní		**KATEDRA**	KKE		**ROK ODEVZD.**	2016

POČET STRAN (A4 a ekvivalentů A4)

CELKEM	65		**TEXTOVÁ ČÁST**	65		**GRAFICKÁ ČÁST**	0

STRUČNÝ POPIS (MAX 10 ŘÁDEK) **ZAMĚŘENÍ, TÉMA, CÍL POZNATKY A PŘÍNOSY**	Diplomová práce je zaměřena na posouzení vlastností řešičů dynamiky turbulentního proudění pro simulaci nestlačitelního proudění v nízkotlaké turbinové lopatkové kaskádě pomocí metody Large Eddy Simulation. Masivně paralelní výpočty byly spuštěny na vysoce výkonných výpočetních systémech. Hlavními nástroji posouzení byly proudové charakteristiky a analýza průběhu výpočtu.
KLÍČOVÁ SLOVA **ZPRAVIDLA JEDNOSLOVNÉ POJMY, KTERÉ VYSTIHUJÍ PODSTATU PRÁCE**	LES, proudový motor, plynová turbína, CFD, OpenFOAM, YALES2, masivně parallelní výpočty, numerická simulace

Prohlášení o autorství

Předkládám tímto k posouzení a obhajobě diplomovou práci zpracovanou na závěr studia na Fakultě strojní Západočeské univerzity v Plzni.
Prohlašuji, že jsem tuto diplomovouou práci vypracoval samostatně, s použitím odborné literatury a pramenů uvedených v seznamu, který je součástí této diplomové práce.

V Plzni dne 20. května 2016. .....

Declaration of authorship

By this I submit the diploma thesis written in the end of my studies at Faculty of Mechanical Engineering of University of West Bohemia to be revisited and defensed.
I proclaim that I have made this thesis on my own, with the use of literature and other sources listed inside the thesis.

In Pilsen, 20$^{\text{th}}$ May 2016. .....

Acknowledgements

I am grateful to many persons which helped me to finish the work on this thesis.

Prof. Laurent Bricteux fairly deserves to be at the top of this paragraph. He accepted to supervise my thesis which was written on my Erasmus stay at University of Mons, Belgium, with all its obstructions and limitations it had. Those including not being the only one official supervisor and letting me continue my work in distance after returning back home to Pilsen, communicating in English all the time and so on.

Ing. Roman Gášpár at my alma mater was ready to comment, review and advise on a thesis of a subject that he did not design, hence I appreciate his effort too.

I thank everyone that made the mentioned exchange visit possible and also very joyful, including my new friends from around the world, the coordinators and international offices and the kind and helpful staff at Fluids–Machines Department of University of Mons.
Last but not least, my heartfelt thanks goes to my family and my love Magdalena. They support me in every way they possibly can in my studies and far beyond.

Contents

Nomenclature

Quantity	**Name**
B [−]	Normalized blade axial/streamwise chord
C [−]	Normalized blade chord
C_w [−]	WALE model coefficient
c_f [−]	Coefficient of skin friction
c_p^D, c_p^S [−]	Coefficient of pressure, different definitions
D [N]	Drag force
ER_{ij} [−]	Mesh cell expansion ratio of j-th cell along i-th direction
F [N]	Force
L [N]	Lift force
h [m]	Finite volume cell dimension
I [−]	Turbulence intensity
i [°]	Angle of incidence
k [m^{-1}], [J, /kg^{-1}] [−]	Turbulent vortex wavenumber, turbulent kinetic energy, normalized
l [−]	Normalized characteristic turbulent length scale
$\dot{m}$ [$\mathrm{kg\,s}^{-1}$]	Mass flow
p [Pa] [−]	Pressure, normalized pressure
r [m]	Radius
S [−]	Normalized blade cascade pitch
S_{ij} [s^{-1}]	Strain rate tensor
t [s] [−]	Time, normaized time
u [m s−1] [−]	Flow velocity, normalized
u^* [m s−1] [−]	Friction velocity, normalized
u' [m s−1]	Velocity fluctuations
W [$\mathrm{J\,kg}^{-1}$]	Mass specific work
Y_p [−]	Coefficient of total pressure loss
X, Y, Z [m] [−]	Curvilinear wall fitted coordinate components, normalized
x, y, z [m] [−]	Cartesian coordinate components, normalized
x^+, y^+, z^+, X^+, Y^+, Z^+ [−]	Dimensionless and case specific normalized wall distances in respective directions

Quantity	**Name**
$Co\,[-]$	Courant number
$Fo\,[-]$	Fourier number
$Ma\,[-]$	Mach number
Re, $Re_h\,[-]$	Reynolds number based on C, based on h
$\alpha_1\,[^\circ]$	Blade design inlet angle
$\alpha_2\,[^\circ]$	Blade design exit angle
$\alpha_1'\,[^\circ]$	Flow inlet angle
$\alpha_2'\,[^\circ]$	Flow exit angle
$\alpha_m\,[^\circ]$	Angle of ideal flow mean velocity
β, $\gamma\,[-]$	Taylor series expansion coefficients
$\delta_{ij}\,[-]$	Kronecker tensor
$\epsilon\,[\mathrm{m^2 s^{-3}}]\,[-]$	Turbulent dissipation rate, normalized
$\eta\,[\mathrm{m}]\,[-]$	Turbulence length scale, normalized
$\lambda\,[\mathrm{m}]$	Wavelength
$\nu\,[\mathrm{m^2 s^{-1}}]$	Kinematic viscosity
$\Omega\,[\mathrm{rad\,s^{-1}}]$	Angular velocity
$\omega\,[\mathrm{s})^{-1}]\,[-]$	Specific turbulent dissipation rate, normalized
$\rho\,[\mathrm{kg\,m^{-3}}]\,[-]$	Density, dimensionless density
$\tau\,[\mathrm{Pa}]\,[-]$	Shear stress, normalized
$\theta\,[^\circ]$	Blade camber angle
$\zeta\,[-]$	Zweifel blade loading coefficient
$\xi\,[^\circ]$	Blade stagger angle

Subscript	**Meaning**
1, 2	Inlet, outlet
0, d, atm, ref	Total, dynamic, atmospheric, reference (pressure)
i, $j\,[-]$	Universal indices
id	Ideal
m	Mean in space
min, max	Minimum, maximum value
r	Radial
w	Wall

1 Introduction

During the last decades, the design of turbomachinery started to account for phenomena, which were mostly neglected before. Aside from uncertainty analyses underwent to describe off-design operation, the effects of unsteadiness of the flow were considered too. Many of these advancements were made available thanks to development of hardware and software capable of complex numerical simulations, especially in the field of *The Computational Fluid Dynamics (CFD).*

There is a wide variety of codes used for computations in CFD, some of them also fairly optimized to help research, design and design verification in turbomachinery applications.

The work presented in this thesis concentrates on assessing some of the approaches to computational analysis of a flow inside a low pressure gas turbine blade cascade.

Cascade tests, both experimental and computational, are traditional way to examine blade profiles for axial turbomachines. They give limited amount of information about an actual turbine (or compressor) performance, but it is often capable of defining the profile losses - a significant part of losses affecting total efficiency. Generally speaking, cascade tests are steady flow cases, but there are also efforts put to capture unsteady flow features natural to turbomachine operation. Incompressible flow is considered, which is known to be a sufficient approximation for two-dimensional turbine cascade flow.

Computational methods arose, that can evaluate the design of all the angular blade rows in a axial turbomachine altogether. They are capable to capture most of the phenomena in a real turbine (or compressor), but always as time averaged steady flow results. When one wants to calculate profile losses, omit moving or static wall interactions and look into the mechanisms of boundary layer transition and separation, possibly introducing unsteady boundary conditions, sticking to *Large eddy simulations (LES)* on a periodic 3D channel is a reasonable decision.

It is capable of capturing unsteadiness in fine enough resolution using arguably affordable computational time and power. This type of simulation is the keypoint of a prismatic low pressure turbine cascade flow computational examination as performed by author and reported on the ongoing pages. For comparisons, steady RANS *(Reynolds-averaged Navier-Stokes)* simulations were also underwent, besides the wide range of results obtained from other authors working with the T106A cascade.

High performance computing (HPC) setups are the inevitable need to perform such analysis. Still, the flow conditions imposed are quite off-design, since the memory and CPU cost increases with the flow velocity or Reynolds number respectively. The results still represent an insight into boundary layer phenomena and unsteady influences. Several facilities of a consortium of high-performance computing centers of Belgian universities - *Consortium des Équipements de Calcul Intensif (CÉCI)* were used.

Both high performance, high discretization order academic solver YALES2 and more conventional OpenFOAM CFD package were used, both capable of feasible massively parallel computing. Common cascade performance indicators were obtained and correlated with each other and accessible references. The phenomena of fluid dynamics are then discussed and the approaches undertaken by the software tools and authors' ways of their usage is described and compared.

2 Literature review

The mentioned blade profile T106A was used to design and manufacture the low pressure turbine of Pratt & Whitney PW 2000 aviatic jet engine series, see chapter 2. It has entered operation in 1984 already [15], but it still represents the most numerous type of modern engines - high bypass multi-spool configurations, where the design of low pressure turbine stages driving the fan is crucial for achieving a competitive product.

In the low pressure turbine the last part of expansion occurs, where the flue gas is already

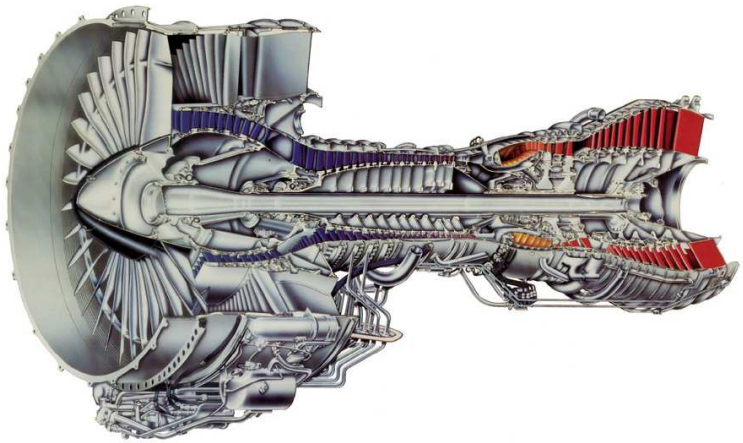

Figure 1: The PW2000 jet engine, image courtesy of Pratt & Whitney, A United Technologies Company

of low density. In spite of that, its turbine spool needs to deliver the biggest fraction of energy to the thrust generating fan. Therefore these turbines are large multistage assemblies weighting a significant amount of total engine mass. The modern design trends, observable also in PW 2000, are thus oriented into reducing the weight, which is mostly achieved by using high loaded blades like T106A. These blades usually are also widely offset from each other - the pitch to chord ratio is high. Their high flow turning angle with wide interblade channels pushes the natural capabilities of flow in a convergent turbine channel to stay attached to the blade surface to the limit.

The above mentioned facts lead to conclusions such that profile losses are the most significant amongst all, when the blades are of large span to chord ratio and there is a relatively high risk of flow separation. The next chapter 2.1 describe the basic theory of turbine cascades and gives background to the analysis of all quantities of interest in order evaluate the performance of the cascade. Next, the scope is turned to to CFD techniques used throughout this work in chapter 2.2.

2.1 Fluid dynamics of turbine cascades

Main purpose of 2D cascade tests is to determine the profile loss and blade row performance. It is an important part of a turbine design, but it concentrates on a single stator or rotor blade row, classically even only on a prediction of performance of just one section of a twisted blade. It cannot tell the effects of hub-blade boundary layer interaction and tip clearance effects nor it simulates flow in radial direction or leakage flows. It helps to design or evaluate the profile of the blade and test the off-design conditions performance as well.

The flow is considered 2D and periodic over each blade of the row, which can be odious task to achieve on an experimental equipment, but it has been figured out a long time ago. Despite that, the periodic behavior eases the computational approach and allows to apply periodic boundary conditions inside the interblade channel. The fact that turbulence is always three dimensional is often omitted for low-fidelity mathematical flow models such as RANS or inviscid Euler simulations. Unfortunately, the solution of LES on a 2D domain is not physical. So even though one performs 3D LES transient simulations, the goal is to find a solution of a pseudo-steady and, from the overall point of view, two-dimensional flow. In this manner, LES is much closer to real world experiments on a cascade than RANS.

A cascade geometry is described by chapter 3.1 in chapter 3 since the actual geometry of studied blade profiles is applied. The definitions of inlet and outlet velocity, design inlet and outlet angles α_1, α_2 as well as flow inlet and outlet angles α'_1, α'_2 and all the essential blade geometry parameters are clear from the figure. The angles are taken as being oriented counter-clockwise from the x-direction. $\alpha_1 = \alpha'_1$ because the angle of incidence $i = 0$ is imposed exclusively in this thesis. In incompressible flow, the x-component of velocity, analogical to axial component in an angular blade arrangement, remains constant unless the channel is thinned in spanwise direction. By this fact, very clear sight of relations between losses and performance parameters is gained.

2.1.1 Profile losses and blade performance

The profile loss is a combination of inviscid and viscid effects acting on the stagnation pressure decrease. The inertia of inviscid flow and pressure difference between suction and pressure side (driving the rotor blades in a turbine) is also a reason for the overall turning angle of the flow to be always smaller than the blade camber angle. This applies even for a design conditions of inlet angle equal to the metal inlet angle.

When viscous fluid is present, boundary layer (BL) following the no-slip condition at the blade surface is generated. The BL theory tells that a fluid approaching an edge of a stationary flat plate forms a layer of laminar flow near the wall assuring the change of fluid velocity from zero at the wall to the value of free stream velocity. The layer thickens along the flow direction and at a distance long enough from the edge, this layer undergoes a transition into turbulent regime . The thickening has negative influence on the effective flow area due to the velocity deficit along walls. This is resembling the definition of boundary layer displacement thickness, however it is not usually evaluated due to the trouble of obtaining the reference velocity inside a narrow channel containing highly perturbed flow.

Those flow features are combining: on the suction side, the boundary layer thickening is amplified by the inertia effects and the pressure gradient in the back of the blade can become such strong, that boundary layer separates from the surface and a possibly a region of backward facing velocity known as a separation bubble occurs under it. This can happen to laminar BL as well as turbulent ones in spite of the velocity fluctuations in a turbulence flow field can prevent the separation further. It is a major restriction of effective flow area and is about to be avoided as much as possible. The separation bubble is a 3D object and cannot be correctly represented in 2D.

In compressible flow, shock discontinuities also create losses. This is not discussed further, the paper concentrates on incompressible flow.

2.1.2 Pressure coefficient

The distribution of the pressure along the blade surfaces can easily identify separation bubble and other flow features. The normalization can be made in various ways. The definition mentioned in [8] is in equation (2.1).

$$c_p^D = \frac{p_w - p_1}{p_{d1}} \tag{2.1}$$

Steiger uses different definition in his work [14], see equation (2.2).

$$c_p^S = \frac{p_{01} - p_w}{p_{01} - p_2} \tag{2.2}$$

2.1.3 Aerodynamic forces

The lift and drag are part of a common terminology for every airfoil analysis and the meaning is quite straightforward regarding aeronautical wings or slightly curved compressor blades. Unlike those, for high turning turbine blades there is usually a large difference between the direction of lift and the tangential/pitchwise direction. The theory presented here is valid only for low speed turbomachines operating with incompressible flow as the equations presented assume conservation of mass by no change of axial velocity.

First the tangential and axial force is derived from momentum equation on a control volume containing one blade of unit span and two halves of the interblade channel. Lift and drag is projected to respective directions by use of the mean camber angle α_m : $\tan\alpha_m = 1/2(\tan\alpha_1 + \tan\alpha_2)$. The metal angles are used to define α_m and velocities in the figure, therefore the velocities are marked as ideal. Proceeding is clear from equation (2.3) and chapter 2.1.3. The location of the forces is often approximated to be at 25% lenght of blade mean line, here adapted to be at 25% of chord, in x-direction. This may not be accurate assumption, but since the aerodynamic torque is not evaluated, it is pictured just as an illustration.

$$\begin{aligned} F_x &= (p_2 - p_1)P; & F_y &= \rho P u_x^2(\tan\alpha_1 + \tan\alpha_2); \\ L &= F_x \sin\alpha_m + F_y \cos\alpha_m; & D &= F_y \sin\alpha_m - F_x \cos\alpha_m. \end{aligned} \tag{2.3}$$

To obtain dimensionless coefficients, L and D is divided by dynamic pressure based on velocity usually taken at the inlet ($p_{d1} = \rho u_1^2/2$) and blade chord C. The coefficients can be obtained also by summing up the projections of dimensionless differential forces accounted by c_p into their respective directions.

2.1.4 Wake deviation and the exit angle

At the trailing edge, the two BLs meet each other, the pressure difference on the interface yields the deviation of the streamlines from the exit stagger angle in direction pointing along the trailing edge radius from pressure side to the suction side. This has a direct effect on the stage performance as the Euler work equation equation (2.4) presented by Dixon [8] amongst many others describes that. Taking an axial turbine blade passage in meridional plane at radius r moving with angular velocity Ω, the blade profile moves at $u_r = \Omega r$. The force in the tangential direction yielding the power obtained from this section can be evaluated as $dF = \dot{m}(\sin\alpha_1' - \sin\alpha_2')/r dr$, power being $d\dot{W} = dF u_r$.

$$\Delta W = \frac{d\dot{W}}{\dot{m}} = u_r(u_1 \sin\alpha_1' - u_2 \sin\alpha_2') \tag{2.4}$$

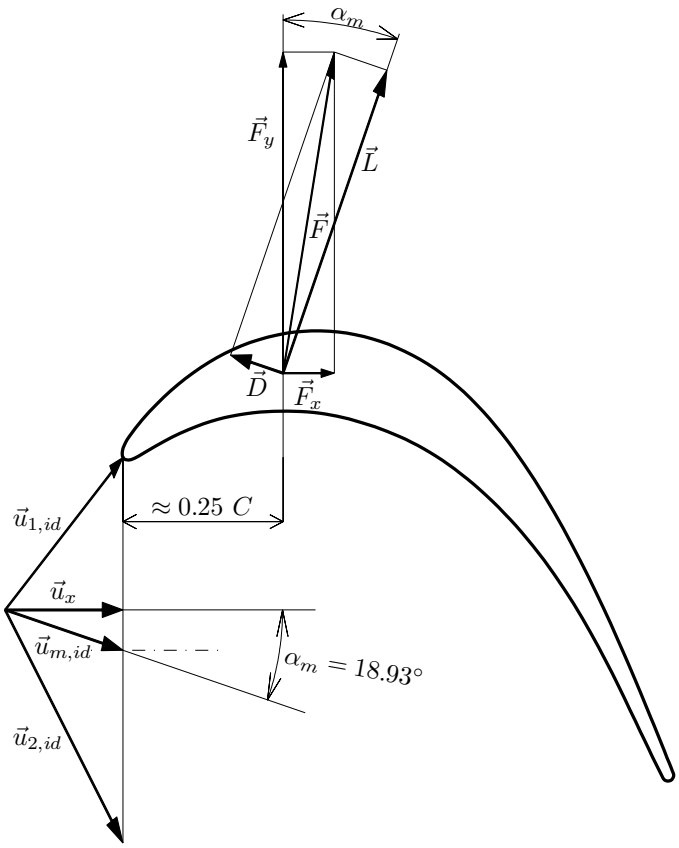

Figure 2: Definition of aerodynamic forces acting on T106A blade profile

The mass specific work ΔW for the operating conditions defined by u_r, u_1, α_1' could then vary only depending on the angle of exit α_2' since $u_2 = f(\alpha_2')$. The bigger the deviation, the bigger the exit angle and the lesser the work and power obtained. The latter presented equations were adapted to give clear sight at the relation between a cascade and an annular rotor passage. There is no power output from static blades of a cascade, but static forces are present and angles measured are valuable. A convenient way to obtain the value of exit angle from measurement or simulation data is to fraction the integrals of tangential and axial momentum over the pitch eg. for cascade rather called streamwise and pitchwise momentum. See following equation (2.5), where a simplification for $\rho = \text{const.}$ is applied.

$$\tan \alpha_2' = \frac{\int_0^P \rho u_x u_y dy}{\int_0^P \rho u_x^2 dy} = \frac{\int_0^P u_x u_y dy}{\int_0^P u_x^2 dy} \tag{2.5}$$

2.1.5 Total pressure loss coefficient

To account for all of the losses in a convenient way, total pressure loss coefficient is introduced. For turbines, the reference point for pressure to make the coefficient dimensionless is the outlet section. The total pressure loss $\Delta p_0 = p_{01} - p_{02}$ is divided by the theoretical pressure drop experienced by expansion from stagnating fluid at inlet thermodynamic state to the the fluid of exit static pressure and the respective speed. The described denominator taken in the sense of dynamic pressure represents the maximum possible velocity reachable by that expansion, which must have been isentropic.

The mean exit pressure value $\overline{p_2}$ could be taken to evaluate the total pressure coefficient or even its pitchwise distribution can be gathered when using the local values of pressure p_2. Then the representative value is weighted by mass flow as shown in equation (2.6) with $\rho = \text{const.}$ applied offhand.

$$Y_p = \frac{\int_0^P (p_{01} - p_{02})/(p_{01} - p_2)\rho u_x dy}{\int_0^P \rho u_x dy} \tag{2.6}$$

When evaluating the same fraction of pressures from the denominatorequation (2.6), with the local spanwise pressure p_l over a line right downstream of blade trailing edge, one obtains a graph telling how the pressure loss is distributed in the wake flow structure, mass flow weighted value is also advisable.

2.1.6 Friction coefficient

While pressure coefficient tells about the pressure distribution along the surface, friction coefficient evaluates the velocity distribution. The wall tangent velocity yields viscous friction and thus generates the wall shear stress $\vec{\tau_w}$ with the direction respective of the velocity. The dimensionless form of it is obtained by dividing by inlet dynamic pressure and static pressure difference. This definition is used by [1]:

$$c_f = \frac{|\vec{\tau_w}|}{p_{01} - p_2} \tag{2.7}$$

The local values of c_f could be used to identify the state of the boundary layer, locate a separation bubble or a displacement of stagnation point.

2.1.7 Conclusions for turbine blading

The fluid is accelerating in a turbine stage. For reactional blading, which is T106A, is this statement valid also for the rotor alone. The channel for subsonic flow is convergent. Despite divergent channels of compressor blading, turbine blades can turn the flow much more without risk of BL separation due to that acceleration. This is also a chance for designers to manufacture engines with less turbine stages or less blades in single stage, especially. Benefits of these possibilities are notable the most in aeronautical applications. The modern blades for low pressure turbine are highly turning, according to velocity distribution, front-loaded blades often takes advantage (see [4]) over aft-loaded profiles due to their ability to avoid BL separation further than the other. Those blades' thickness distribution as well as camber curvature is matching the loading location, but the peak thickness still takes place at less than 30% of the chord. The thermodynamic conditions and present material portfolio allows to not employ cooling.

When channels for cooling air are not present, the trailing edge can be thin. It reduces the channel contraction, but lowers the losses by wake width reduction, which is always more important aspect. The spacing of the blades is made bigger than usual. In the low pressure turbine located in the back of the engine the channel is already reaching its peak width. Therefore it is one of the larges parts of the engine meaning a large fraction of the overall weight. It concludes it to be a subject of possible weight reduction, sometimes even preceded over slight performance deficit.
Engineers use to push the blade loadings to the limit, but the peak performance meeting the design conditions is required from the plane jet engine only at take-off. During cruise, the Re can drop down to 25000 and at these conditions, the suction side diffusion raises and the BL stays laminar and often separates, generating large losses. Research is in progress to prevent these losses effectively and various ways are offered. The present works often assume isotropic and statistically time steady turbulence at the inlet, which could be kind of an oversimplification, as proved by [14]. The periodic passing vortices generated by the stator blade row can suppress the separation by turbulizing the near wall flow, but still, there is no control over this turbulence.

2.2 CFD techniques

The Navier-Stokes equations for momentum conservation are solved. A natural form of these equations can by written as a vector equation (2.8) shown below, while the terms of external body forces (due to gravity, rotation of frame of reference) and viscosity effects in compressible flow are omitted for the sake of presented case.

$$\frac{\partial u_i}{\partial t} + \frac{\partial (u_i u_j)}{\partial x_j} = -\frac{1}{\rho}\frac{\partial p}{\partial x_i} + \nu \frac{\partial}{\partial x_j}\left(\frac{\partial u_i}{\partial x_j} + \frac{\partial u_j}{\partial x_i}\right) \tag{2.8}$$

This equation is valid for dealing with measurements as well as direct numerical simulation (DNS). It captures all scales of turbulence fluctuations down to the $\eta_{min} = \sqrt[4]{\nu^3/\epsilon}$ Kolmogorov length scale. This length scale relates to the wavelength λ_{min}. Therefore, for DNS, mesh cell dimensions must be around $h = \lambda_{min}/2$. Looking from the opposite side, the highest wavenumber eddies captured by such grid is $k_{max} = 2\pi/\lambda_{min} = \pi/h$. In slightly directionally non-regular meshes, the h can be approximated as $h = \sqrt[3]{\Delta x \Delta y \Delta z}$.

As [2] states, the range of k representing the dissipational eddies is $k \in < 0.1/\eta, 1/\eta >$, which implies the wavelengths of $\lambda \in < 2\pi\eta, 20\pi\eta >$.

It is common for DNS simulations setup to keep $k_{max}(h)\eta > 1.5$, which leads to the need of grid spacing $h < \pi\eta/1.5$. This is one of the reasons of excessive computational requirements of such simulations and also the reason why there is a lot of effort spent on development of various turbulence models. They are made to achieve different levels of approximation of the real flow to gather results various engineering analyses.
There are other constraints for space and also time discretization. Those are not based on the turbulent scales, but on the need to sustain the stability of numerical schemes and more strictly the accuracy of the results. They are discussed in upcoming chapter 2.2.1.

2.2.1 Large eddy N-S model

The main idea of LES is to omit only the dissipative scales to reach quite lower requirements on mesh spacing and time step while keeping the exact information about large, energy containing eddies. The energy is transported downwards the spectrum, so large eddies are not affected by the dissipative ones. The model of contribution of dissipative eddies is called the sub-grid scale (SGS) turbulence model. Equation (2.9) shows how it is incorporated inside a Navier-Stokes momentum equation (2.8) presented in beginning of this chapter 2.2. Note that the flow variables, p and u, are approximated by $\widetilde{u}$ and $\widetilde{p}$. The $\widetilde{\bullet}$ operator stands for the truncation due to the lower resolution of the spatial and temporal discretization. Various spatial filters can be used, but most of the codes is written in the favor of filtering the field by grid directly.

$$\frac{\partial \widetilde{u_i}}{\partial t} + \frac{\partial (\widetilde{u_i}\widetilde{u_j})}{\partial x_j} = -\frac{1}{\rho}\frac{\partial \widetilde{p}}{\partial x_i} + \nu \frac{\partial}{\partial x_j}\overbrace{\left(\frac{\partial \widetilde{u_i}}{\partial x_j} + \frac{\partial \widetilde{u_j}}{\partial x_i}\right)}^{\widetilde{2S_{ij}}} + \frac{\partial \tau_{ij}^M}{\partial x_j} \tag{2.9}$$

The additional unknown, τ_{ij}^M is modeled always as $\tau_{ij}^M = 2\nu_{SGS}(\widetilde{S_{ij}})$ and so the approach taken by different SGS models only involves the evaluation of the sub-grid scale eddy viscosity.

Present SGS models allows to coarsen the DNS grid by enlarging the spacing h by factor of 4 to 10. The more coarse is the mesh, the bigger is the challenge for the SGS model and the uncertainty introduced by it. Needless to say, coarsening the 3D mesh four times in every direction means reduction of number of cells by factor of $4^3 = 64$ and coarsening the mesh 10 times means 1000 times less cells, so it is always worthed to think about the capabilities of the SGS model. In industrial applications, bigger ratios are often used as one typically does not need to capture the details of flow in every region.

Smagorinsky introduced a SGS model in 1963. This has become one of the most widely used, either in its original or adapted forms. It is known for behaving well in the freestream regions, but is failing in describing the near wall evolution of ν_{SGS}. One of the promising SGS models retaining the near wall behavior called *wall-adapting local eddy-viscosity model* (commonly abbreviated as WALE) was brought in by Nicoud and Durcos [11], 1999.

2.2.1.1 Sub-grid scale turbulence modeling and WALE approach

This sub-grid scale turbulence is devoted to retain the correct behavior of τ_{ij}^M near the wall. The evolution of this variable depends on the grid truncated velocities. Taking the tensor component corresponding to any direction along the wall, lets say x, and the wall normal y, the $\tau_{xy}^M \propto \widetilde{u_x}\widetilde{u_y}$. By substitution of near wall velocities by Taylor series and taking incompressibility into account by not allowing a wall normal velocity of first order magnitude, for $y \to 0$:

$$\left.\begin{aligned} \widetilde{u_x} &= \beta_1 y + \beta_2 y + \mathcal{O}(y^3) \quad &\Rightarrow \quad \widetilde{u_x} &\propto y^+ \\ \widetilde{u_y} &= \underbrace{\gamma_1}_{=0} y + \gamma_2 y + \mathcal{O}(y^3) \quad &\Rightarrow \quad \widetilde{u_y} &\propto (y^+)^2 \end{aligned}\right\} \Rightarrow \tau_{xy}^M \propto (y^+)^3 \tag{2.10}$$

The outcome of equation (2.10) concludes that the modeled value ν_{SGS} should retain this proportionality while S_{ij} is a constant near wall. In fact, this is a major drawback of Smagorinsky model requiring the need to employ damping functions or dynamic procedures for evaluating global or even local constants. Either way, the common Van Driest damping produces $\nu_{SGS} = \mathcal{O}((y^+)^2)$ and it is still not correct. Every eddy-viscosity based SGS model is defined as following:

$$\nu_{SGS} = C_w \Delta^2 \overline{OP}(x, y, z, t), \tag{2.11}$$

where Δ is characteristic sub-grid lenghtscale, normally $\Delta = h$. For WALE, C_w is real constant, which is not adapted as like in dynamic models. The value has been calibrated for various uses, typical value is 0.325 when using $\Delta = \sqrt[3]{\Delta x \Delta y \Delta z}$ on non-uniform grids. The OP operator is arbitrary and it is always based on an invariant of a tensor related to the strain rate $\widetilde{S_{ij}}$. WALE has been built in terms of equation (2.12).

$$\nu_{SGS} = C_w \Delta^2 \frac{(\mathcal{S}_{ij}^d \mathcal{S}_{ij}^d)^{3/2}}{(\widetilde{S}_{ij}\widetilde{S}_{ij})^{3/2} + (\mathcal{S}_{ij}^d \mathcal{S}_{ij}^d)^{5/4}} \tag{2.12}$$

The caligraphics mark the traceless symmetric part of the original tensor, d superscript indicating the deviatoric part of latter. The numerator part has an exponent of 3/2, which provides the $(y^+)^3$ behavior for $y \to 0$, while the base is proportional to $(y^+)^2$. The physical dimension of viscosity is earned when the first denominator term takes place. The second denominator term goes to 0 near wall, but is of finite value away from it. It is used to avoid division by zero, because the first term alone could cause it.

The nature of WALE model allows also to resolve the boundary layer transition due to the zero eddy viscosity value reached in pure shear flow that imposes no damping to the evolution of unstable waves. But it has been discussed and proved by [3] that WALE is too dissipative to the free vortices and their centers, where the strain rate is negligible, but the rotation rate is not.

2.2.1.2 Time and space discretization

As announced in beginning of chapter 2.2, besides the limitations of mesh spacing related to the turbulent scales, there is also a limit to discretization in both space and time imposed to keep the simulation accurate. The constraint is represented by the fraction written in equation (2.13).

$$\frac{Co}{Fo} = Re_h \cong 1, \tag{2.13}$$

where

$$\begin{aligned} Co &= \frac{u_{max}\Delta t}{h} && < 0.25[-]. \\ Fo &= \frac{(\widetilde{\nu} + \nu_{SGS})\Delta t}{h^2} && < 0.15[-]. \end{aligned} \tag{2.14}$$

These numbers describe the wave propagation. Courant number representing convection and Fourier number standing for diffusion. Diffusion wave proceeds by distance of $\sqrt{\nu t}$ per

time unit.

The described conditions are usually hard to achieve for either DNS or LES of reasonable resource consumption and are not therefore often followed very strictly. See chapters 5.1 and 5.2 describing how they were treated in this particular case.

2.2.2 Reynolds averaged N-S model

Unlike the spatially filtered equations for LES, RANS equations are averaged in time. Therefore there is an obligation to model the whole spectrum of turbulent fluctuations. During the analytical process of averaging, new unknowns are produced by terms which contain product of correlated varying quantities. Taking the basic equation (2.8), one obtains the following:

$$\frac{\partial \overline{u_i}}{\partial t} + \frac{\partial (\overline{u_i}\overline{u_j})}{\partial x_j} = -\frac{1}{\rho}\frac{\partial \overline{p}}{\partial x_i} + \nu \frac{\partial}{\partial x_j}\left(\frac{\partial \overline{u_i}}{\partial x_j} + \frac{\partial \overline{u_j}}{\partial x_i}\right) - \frac{\partial \overline{u_i' u_j'}}{\partial x_j} \tag{2.15}$$

As the last term accounting the force action of turbulence per unit mass, according to [9], one can substitute:

$$-\overline{u_i' u_j'} = \nu_t \left(\frac{\partial \overline{u_i}}{\partial x_j} + \frac{\partial \overline{u_j}}{\partial x_i}\right) - \frac{2}{3}\delta_{ij} k \tag{2.16}$$

This way, eddy viscosity ν_t and turbulent kinetic energy $k = 1/2\ \overline{u_i' u_i'}$ are introduced. Note that ν_t can be factored out together with ν.

The approach described by equation (2.16) is called eddy viscosity model. It is less complex than the second option - the Reynolds stress transport model - which is not used often due to its high resource consumption while carrying the drawbacks of RANS equations.

2.2.2.1 $k - \omega$ *SST* turbulence model

Many ways to model ν_t and k were designed. One of the most advanced models in treating flows with or without separation of the boundary layer, achieving good results in resolved near-wall regions as well as in the freestream is the *shear stress transport (SST)* $k - \omega$ model. It comes out of a range of two-equation linear eddy viscosity models widely used for general applications. It has been numerously modified to enhance performance and a major revision by original author, Menter, was made in 2003[10]. This version is the

current one used by most CFD codes including the ones used by author and is presented here. The turbulent viscosity is formulated like

$$\nu_t = \frac{a_1 k}{\max\left(a_1\omega, SF_2\right)}, \tag{2.17}$$

where $S = \sqrt{S_{ij}S_{ij}}$, the invariant measure of the strain rate. F_2 is a blending factor and a_1 a calibrated constant. Turbulent kinetic energy k and specific dissipation rate ω are evaluated from transport equations which are partial differential as N-S equations. Those two equations and their respective transported quantities are closing the problem of RANS equation set by replacing the need to evaluate the covariance of fluctuations. Those transport laws involve another blending factor, a production rate limiter and large number of calibrated constants. The blending factors system allows "switching" of approach between $k-\omega$ in the wall boundary layers and $k-\epsilon$ in the freestream. This is to avoid the initial condition sensitivity of the original standalone $k-\omega$ invented by Wilcox.

3 Case setup

An important note is made here: The case is built in a way, that it uses the dimensionless unit blade chord $C = 1$ and dimensionless inlet unit velocity $u_1 = 1[-]$ as a norm for all other quantities to be taken as like they are dimensionless too. While this is used throughout the thesis, no special notation is used and unit labeling is omitted. The author hopes that it odes not cause any misunderstandings.

3.1 T106 blade profile

As mentioned and discussed in previous chapters, the blade profile T106 is intended to be used for fabrication of gas turbine blades, especially for rotors of low pressure stages. As usual for a gas turbine blading, the channel between those blades is convergent, therefore the stage is a reaction one, absolute gas velocity increases by passing through this stage. The profile is high cambered, both the inlet angle and the outlet angle are relatively high. It follows the design trend of high loaded blades on which comments were made before.

The profile is suitable to analyze the state-of-art blade design techniques, which are still based exclusively on steady phenomena. Undergoing an unsteady flow simulation should allow to point out the influences of unsteady flow structures on the blade performance.

For convenience, the blade profile was geometrically represented "as is", so it is dimensionless, while taking the blade chord length as unity. The data were obtained from [14] in so called Selig format - first point of data is the trailing edge and sorted points along suction surface follow to the leading edge, then pressure surface points from leading edge to trailing edge are written. This is how the format was intended to be used, however the definitions of the trailing edge and leading edge used for wing airfoils are ambiguous in case of highly curved turbine blading. A simple script was used to find the coordinates of the edges in favor of design flow angles approach and exit points and the points were split to sets for each blade side and reorganized properly.

3.2 Prismatic blade cascade

The studied cascade comprises of prismatic blades commented right above. The pitch of blade row is taken the same as in the case of Steiger [14], taking into account the ratio of dimensionless distances used by author and Steiger's real physical dimensions. The ratio of the axial chord and the pitch (space) is characteristic for incompressible flow through low

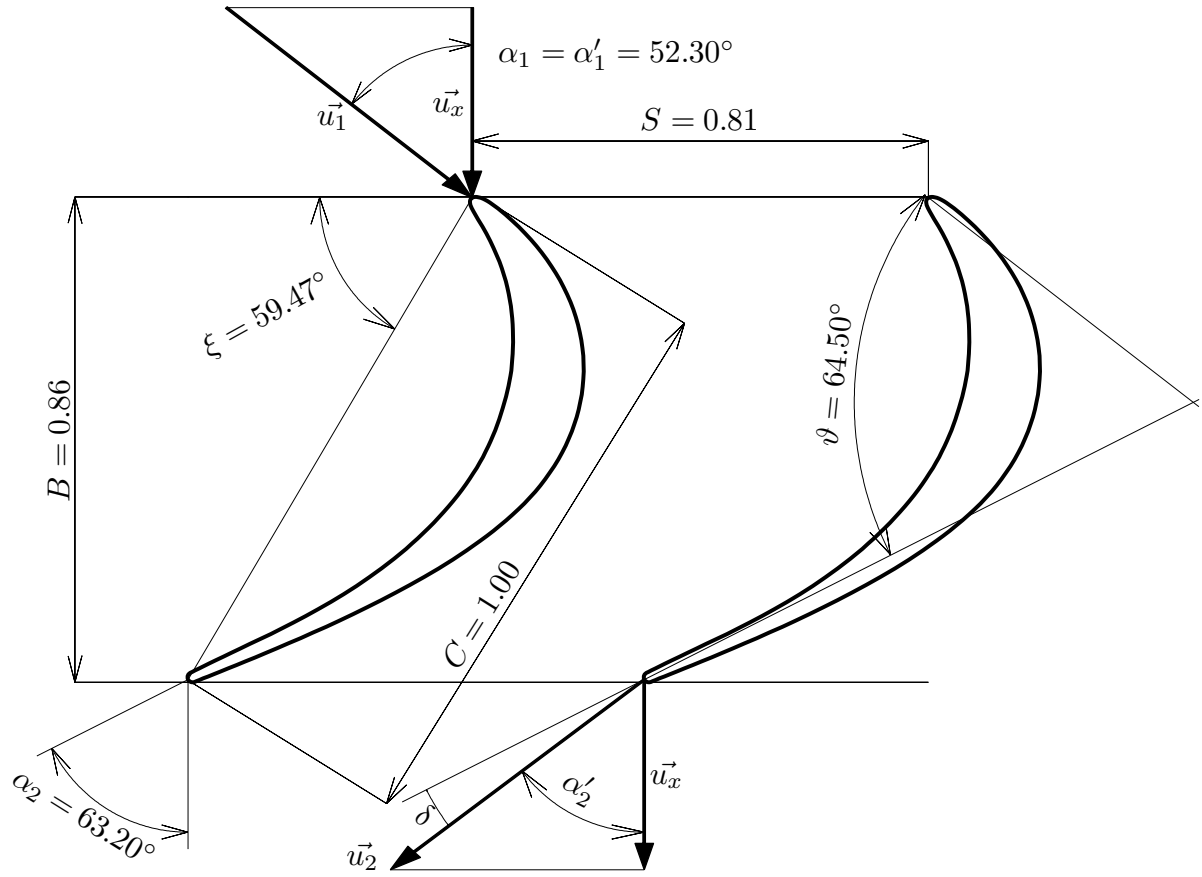

Figure 3: T106A cascade geometry and vectors of real inlet and outlet velocity: $\vec{u_1}$ and $\vec{u_2}$; and their common constant x-component $\vec{u_x}$

pressure turbines of jet engines as it can be derived from Dixon's and Hall's [8] comments on Zweifel criterion.

This criterion states that the ratio of actual to ideal blade tangential load should be around 0.8, but can exceed the value of 1 in the case of modern LP gas turbines. The increased width of the channel resulting in a decrease of flow guidance and increase of danger of boundary layer separation is balanced by weight reduction reached when using less high loaded blades.

$$\zeta = 2 \cdot \frac{P}{B} \cdot cos^2\alpha_2 \cdot (tan\alpha_1 + tan\alpha_2) = 1.04\,[-]. \tag{3.1}$$

The actual value obtained by evaluating the expression in equation (3.1) above shows that the pitch value used for analysis is reasonable.

3.3 Computational domain

The flow field in experimental cascades is intended to be periodic, at least in a way that the quantities measured on the middle airfoil are close to values which would be measured on a truly periodic cascade - theoretically the one with infinite blade count. The outcomes of cascade analysis, experimental or computational, are the properties of the blade profile.

Therefore, there is no need for a computational domain to contain more than one pressure side and one suction side of the airfoil. Obviously, there are two ways to fulfill this requirement. The domain could be taken as a channel between two blades, enclosed by the no slip wall boundaries on top and bottom, which continues some distance in front of leading edges and trailing edges as a periodic boundary. The second way, which is exclusively used throughout this work, is to split two channels in half and enclose one blade profile between two boundaries periodic in their whole length. This approach eases the visualization of boundary layer all around the blade and allows the expected vortex street in the wake not to be split by the boundary. There is still a possibility to view what is happening along the channel width when the domain is replicated in post processing and visualization tools.

Speaking of the pitchwise periodicity, there are few parameters of the boundaries presented to comment on. Those boundaries are prolongated in streamwise direction to avoid the strict inlet and outlet boundary condition to influence the flow regions of the biggest interest. In the back of the blade the prolongation purpose is also to visualize the wake. Inlet plane is located one chord distance in front of the blade's leading edge. The outlet lays as far as 3 chords behind the trailing edge for unstructured mesh according to chapter 4.2 and 2.5 chords for structured mesh described in chapter 4.3. The domain boundaries follows the design flow exit direction for a certain distance behind the blade and are then turned to axial direction to avoid skew of outlet and to lower the pitchwise overall dimension of the domain.

The spanwise periodicity is imposed for LES for a clear reason: It computes directly a part of the turbulence spectrum, so the simplification of the simulation by using 2D domain is not possible. The turbulence is three dimensional by nature. The spanwise dimension have to be long enough to capture the longest wavelengths of turbulent perturbations. In preliminary computations excessively large numbers of points were avoided - a short domain of 25% of blade chord in spanwise direction was used. Production runs were then launched on a domain span over double the length of chord to ensure that even the longest wavelengths will fit in this span and no truncation of spectrum will be made. Such domain

is illustrated in chapter 4.3.

The curves defining the channel for unstructured mesh were obtained from the NUMECA's turbomachinery meshing tool AutoGrid and were exported to use with other meshing tools designed for general, unspecialized use. More on this topic in chapter 4.2.

For structured mesh domain was shaped manually and imported to ICEM CFD with the help of MATLAB/GNU Octave script. It is further discussed in chapter 4.3.

3.4 Mathematical model

3.4.1 Flow conditions

The real flow in experimental cascade is an approximation of a flow in the real turbomachine and can be made to meet various requirements. The dimensional analysis allows to study flow of air instead of actual flue gas in a turbine, which is a homogeneous mixture of diatomic (N_2) and polyatomic (CO_2, H_2O) gases. For real-world experiments analogical to authors' simulations setup (see chapters 3.4.2 and 3.4.3) and the thermodynamic properties of either air or flue gas, $Ma < 0.2$ always. The expansion in a real turbine is close to the adiabatic state change. In the cascade, where no work is being output, the process is near the ideal isothermic one. Differences of the state parameters of real cascade flow are negligible when observing only the characteristics related to the movement of the gas mass.

The phenomenon approximated by the simulations is taken as an incompressible viscous isothermic flow of one phase Newtonian fluid. This is believed to be an accurate representation of the conditions described right above. The isothermic characteristic is advantageous because it allows to omit the employment of the N-S energy equation. The Newtonian model of viscosity is proven to be valid for working fluid of both cascades and gas turbines.

Two general approaches to solve Navier-Stokes equations were used. First, The Reynolds averaged equations are utilized to capture the flow in a steady manner. As the influences of the unsteady nature of the turbulent flow and time changes in the turbulence field around the blade were discussed before, the unsteady computations using the large eddy turbulence modeling is performed as the key part of this work.

The present simulations are carried out with $Re = 10^4$, which is sufficient to fully characterize the incompressible flow. The value is too low to obtain comparison for a turbine

operating conditions involving the off design operation. The boundary layer is expected to undergo a separation in the aft part of the suction surface. Turbulization and possible reattachment of wall boundary layer were intended to be studied. The mentioned Re is based on the characteristic dimension being the chord length and the inlet flow velocity. The dimensionless definition is constructed to control Re by changing the molecular kinematic viscosity ν. For the present value of Re:

$$\left.\begin{array}{lll} u_1 = |\vec{u}_1| & = 1 & [-] \\ L = C & = 1 & [-] \\ \nu & = 10^{-4} & [-] \end{array}\right\} \quad Re = \frac{L\,u}{\nu} = 10^4\,[-] \tag{3.2}$$

Density, remaining as the last non-defined variable of an isothermic viscous incompressible flow, is not constrained and could be set arbitrarily. To make the post-processing convenient, the value is set to unity: $\rho = 1\,[-]$. As it may be clear from the last few sentences, no equations or tables of thermodynamic parameters of fluid are employed since the Reynolds number is the only characteristic value for truly isothermic incompressible flow.

3.4.2 Boundary conditions

There is a need to prescribe the behavior of every single flow variable on the domain boundary, either natural - p and u or the ones introduced by turbulence modeling. A well-posed problem is a term describing the configuration of BCs.

The simplest part of the BCs setup are the patches normal to transverse and spanwise direction. They are periodic, also called cyclic, and represent the replication of the domain flowfield. Then, the vectors, gradients and waves pointing out of one of the domain sides are extrapolated to point inside the domain on the opposite side.

3.4.2.1 Velocity inlet

All three components of velocity vectors are prescribed on the inlet patch to determine the angle of attack and the magnitude of velocity. Pressure waves in an incompressible flow propagates at infinite speed in all directions, so it can be propagated to the inlet patch assuming it is prescribed at the outlet. Turbulent quantities are imposed at the inlet as well, because those quantities relates to velocity and propagates mainly by the dominant convection.

$$\begin{aligned} \alpha_1' &= 37.7 && [^\circ], \\ |\vec{u_1}| &= 1 && [-], \\ \vec{u_1} &= [\cos\alpha_1', \sin\alpha_1', 0] \cong [0.791, 0.612, 0] && [-]. \end{aligned} \tag{3.3}$$

For LES runs submitted to solver YALES2, an advantage of precomputing a box of homogeneous isotropic turbulence on a small mesh was taken to superpose it to the above described fixed inlet. By this, more physical boundary condition is imposed. The input values for this operation are the same as noted in paragraph 3.4.3.1.

3.4.2.2 Pressure outlet

A constant value of static pressure is prescribed at the outlet patch. According to the fact that almost every CFD code utilizes a paradigm of reference eg. operating pressure, the explicit value of static pressure set at the outlet is playing role of an addition and could be safely set to $p_2 = 0\,[-]$. Reference pressure is an arbitrary non-zero positive value, which kept its default value as an atmospheric pressure $p_{ref} = p_{atm} = 101,325\,[-]$ although there is no logical nor physical background behind it in dimensionless space. The outlet is obviously a location of minimum of total pressure averaged over pitch and by leaving the value of p_2 none above the reference, the static pressure difference is obtained explicitly as a static pressure at the inlet.

The velocity is expected to be always pointing out of the domain through the outlet patch, what allows extrapolation. In spite of that and the fact that the outlet is quite far away form the blade perturbing the flow, there still could be a problem of backflow in early stages of LES runs causing them to explode. This danger takes place at time of turbulent structures development, when the transient solution is not yet physical. A large vortex is usually "washed away" from the blade which causes a negative value of u_x directly causing nonconservative behavior. To prevent this, a conditional BC was imposed that computes the required local backflow from pressure gradient as a patch normal velocity vector field. This regime is not active in the time interval of averaging for results output.

3.4.2.3 Blade surface

The wall surface is a simple static no-slip wall telling that $\vec{u}|_{Y=0} = \vec{0}$.

The pressure is determined by its wall normal gradient, which is zero, as it can be proved from substituting respective zero values for velocity and its first and second derivatives into momentum equation built in curvilinear space fitted to the wall surface. As the velocity

values are zero and constant along the wall, time derivative is zero. First and second velocity derivatives in wall tangential directions are zero because the values of velocity are zero and constant all over the wall. First derivative in the wall normal direction is zero as well to satisfy continuity equation. The second derivative in wall normal direction is zero too because of the zero and constant wall normal velocity component in the laminar sublayer present over a hydraulically smooth wall. With all velocity derivatives put into wall-normal component of momentum vector equation, it reduces to $\frac{\partial p}{\partial Y} = 0$. This allows the solution of Poisson pressure equation by safely extrapolating the unknown wall boundary pressure from the cells adjacent to the wall. All of that is valid if the cells adjacent to the wall are located in the laminar viscous sublayer, which is true for this case as told in chapter 4.

3.4.3 Initial conditions

When no preliminary computations available, the prescribed boundary values were propagated over the whole domain. This is of course a solution irrespective of any physics and it has to be a subject to some kind of treatment before pushing the values into modern and complex RANS an LES solvers. A few iterations of potential flow solver are carried out to align the streamlines better with the geometry. This is done in a blink of an eye on present machines. The output of this marginal computation is treated as a set of zero time initial conditions. The potential simulation gives solutions only for p and u, the turbulent properties initialized as constants on an streamline aligned field make no difficulties to convergence of upcoming viscous flow simulation.

3.4.3.1 Turbulence properties

Values needed for turbulence modeling closure vary with used turbulence modeling approach. As long as they are always used to enclose the same system of equations, they are tightly coupled. Construction of a consistent set to pick the values needed for different models is possible. An assumption, a qualified guess, must be made. Based on the fact, that cascade is an approximation of a turbomachinery flow, a relatively high level of turbulent intensity $I = u'/u = 0.05\,[-]$ is supposed. Based on experiments with periodic bar passing discussed in [14] and their dimension, a turbulent inlet lenghtscale is hold as $l = 0.0102\,[-]$ in the dimensionless space.

Turbulent kinetic energy k and specific dissipation rate ω has to be determined for SST $k-\omega$ RANS calculations. Assuming isotropic turbulence, process of determining turbulence parameters with values of I, u yet mentioned is described in rows of equation (3.4).

$$\begin{aligned} k &= \frac{3}{2}\,u'^2 = \frac{3}{2}\,(I\,u)^2 &&= 3.75 \cdot 10^{-3} \quad [-] \\ \omega &= \frac{\sqrt{k}}{l} &&= 2.026 \cdot 10^{-3} \quad [-] \end{aligned} \tag{3.4}$$

Eddy viscosity ν_t is required for LES without precomputed turbulence. An assumption was made about the eddy viscosity ratio $\nu_t/\nu = 1\,[-]$. This stands for a low turbulence flow expected. The ratio of 1 means that same amount of energy is being dissipated by laminar shear stresses and the turbulent Reynolds stresses as well. This ratio rises to order of hundreds for fully turbulent flow.

4 Grid generation

4.1 Mesh quality requirements

The creation of the computational grid for spatial discretization of the flow domain, usually called mesh, was treated with several approaches and expectations. First a comment over a general technique used exclusively for every version of the grid is made:

The design of the mesh was treated as 2D case of the spanwise normal section of the periodic cascade channel. To obtain a 3D domain, a simple extrusion by arbitrary uniform spacing is made, creating a certain number of identical layers. This way the cells are always prismatic. For the strategies used for meshing here, the mesh consist either of hexahedral elements or triangle base pentahedral prisms. Chapters 4.1.1 to 4.1.3 present general comments and mesh requirements, chapters 4.2 and 4.3 describe the details of different mesh type setup and genration.

First intentions were to design a fully structured multiblock grid to gain advantage of its simple data structure. The implementation of solvers operating such geometrical entity is easier than for unstructured approach and for the codes utilized here, it means also a higher order of accuracy in space. It is always more difficult to asses this kind of discretization, because it involves a large amount of user interaction and parameter input from the user of grid generation software. It is common to use structured grid for turbomachinery internal flow simulations, but it is far easier to retain the mesh quality when wrapping cells over blades lower staggered than T106A and using a channel such short streamwise as it is in a real multistage axial machine. Therefore an unstructured grid was also generated to have a working version in a reasonable time frame and later a possibility to compare results and simulation runtime parameters.

There are main parameters used to describe the mesh quality overall, with only a weak relation to its application and also parameters, which has to be carefully checked for every specific flow problem solved. They are discussed in following paragraphs. When discussing the constraints related to one of the specific simulations, these apply to all of the others. Only one mesh for every RANS + LES simulation pair was used since the most tedious restrictions relates to LES and yields all the difficulties there and not in RANS. The LES optimized mesh is not overly fine for wall resolved SST $k-\omega$ RANS simulations of low Re flow.

4.1.1 Expansion ratio

The mesh has to have smooth transition among neighboring cells size eg. their dimension in every physical dimension separately. If a non-smooth transition is made, the spatial discretization scheme could decrease its order of accuracy. The expansion ratio for every mesh cell of the total count N could be expressed as follows:

$$ER_{ij} = \max\left(\frac{h_{i,j}}{h_{i,j+1}}, \frac{h_{i,j}}{h_{i,j-1}}\right), \text{ for } i = \{x,\ y,\ z\},\ j = 1...N. \tag{4.1}$$

General requirements are to keep the expansion ratio over all of the cells below the value of 1.1 [−], For LES, more strict rule of value of 1.05 [−] in the areas of expected large gradient is imposed.

4.1.2 Aspect ratio

Every cell of the mesh needs to keep the ratio of every pair of its dimension under certain threshold. This maximal acceptable value is mostly solver-specific. For the used mesh extrusion extrusion strategy the most "stretched" cells are the smallest ones on the wall boundary. Those are constrained by LES requirements for first near wall layer not only in wall normal direction as usual, but also spanwise and streamwise in terms of presented case. These constraints are more tight than most solvers' expansion ratio thresholds and are therefore commented further in chapter 4.1.5. A large spanwise aspect ratio can also occur in far field regions, but due to the constraints introduced by multiblock strategy described in chapter 4.3 it is also almost impossible to reach critical values.

4.1.3 Skewness

Skewness is in other words the orthogonality of the hexahedral cells or the factor of sustaining the inner angles as close to the cells' originating regular polyhedron as possible. It has several definitions for many kinds of cells. High skewness should be avoided especially in the regions of large gradients again.

The skewness of cell faces oriented along spanwise direction is not a concern due to simple operation of extrusion. For triangular face prisms, low skewness is ensured by the large number of degrees of freedom with which the generation algorithm operates.

Skewness was discovered as the most limiting quality measure for the hexahedral mesh. Improving skewness was very time consuming and caused divergence in some preliminary computations.

4.1.4 Periodic points coincidence

Options of launching simulations on underlying meshes with non-coincident periodic boundaries exist, but the interpolation can lead to non-conservativeness or a loss of result accuracy. The YALES2 solver cannot handle non-conformal interfaces anyways. The location of the points is therefore synchronized all the way along the channel limiting curves. Extrusion again yields correct location of points on the spanwise periodic patches and equal spanwise spacing over tranverse normal patches. Only the equal number of points and identical laws for their spacing has to be set as generation input concerning periodicity. However, in ANSYS ICEM CFD interface, an explicit vector for extrusion had to be set rather than detection of the face normal direction automatically. The latter caused crucial point coordinates inaccuracy, preventing the resulting spanwise boundaries from linking to each other.

4.1.5 First wall adjacent cell layer

The mesh in the boundary layer is often described by the first cell layer thickness assuming a satisfaction of previously written conditions, chiefly the expansion ratio. An abstracted way to define this thickness is to set it in a dimensionless wall distance $y^+ = u_* \, Y/\nu$ of recommended value. The proceeding is clear from equations (4.2) and (4.3). The value recommended by Menter for his own SST $k-\omega$ model [10] without wall functions is $y_w^+ \leq 2$, for wall resolved LES it is $y_w^+ \leq 1$. The difference here is not such big for separate grids design to be reasonable.

$$c_f = [2\, log(Re) - 0.65]^{-2.3}, \qquad \tau_w = \frac{c_f \rho u_\infty^2}{2}, \qquad u_* = \sqrt{\frac{\tau_w}{\rho}}. \tag{4.2}$$

$$\Delta Y_w = \frac{y_w^+ \nu}{u_*} \cong 1.5 \cdot 10^{-3} \tag{4.3}$$

To be able to evaluate the wanted value, an approximation of the friction coefficient c_f has to be made. The relation presented in the first identity of equation (4.2) is a result of Schlichtling's research of a flat plate validated for $Re < 10^9$ [13]. The velocity profile obtained this way is vaguely approached and back check must be done if the $y_w^+ = 1$ condition was fulfilled all along the blade surface. An iterative process of mesh generation may

be required.

For LES, there are requirements for the resting two directions too. They arise from the 3D nature of turbulent velocity fluctuations. [12] recommends $\Delta x_w^+ \in \langle\, 50,\, 150 \,\rangle$ and $\Delta z_w^+ \in \langle\, 15,\, 40 \,\rangle$. This also plays a role of sufficient cell aspect ratio limit and directly determines the extrusion direction. More comments are made in next two chapters respective to the mesh types.

4.2 Unstructured prism mesh

As a first option, design of a surface triangle mesh with spanwise extrusion for 3D LES was chosen. As every type of unstructured grid, it does not require laborious setup. The domain was taken from the first tries on multiblock structured mesh creation in AUTOGRID software, which were unfortunately nonsuccessive due to limited options of automated topology design, extensive requirements on wake prolongation and also author's brief experience with the tool.

In ICEM CFD, the domain edges including blade contour and curves for the support of an O-grid around blade were discretized and a tetragon with prescribed finer spacing was added in the back of the blade. There are not many options how to control the surface mesh generation process, but the resulting mesh based on edge spacings and first wall adjacent layer thickness of $0.0015\,[-]$ were sufficient to obtain a quality grid. See chapter 4.2.

The 2D triangle structure has a drawback of almost no option of stretching the cells along any of two directions. Due to this fact, large number of points are laid along the airfoil curves. Often a hybrid meshes with triangle-tetrahedra interface are made, but it suits external aerodynamics cases better because of the possibilities to join the regions far enough from the walls, where the side of triangles could match the width of tetrahedra without being too skewed or creating too coarse grid. An example of fully unstructured grid in a case similar to this thesis is [7].

The final mesh is of very high quality in terms of all the subsequent sections of chapter 4.1, except y_w^+ criterion, which is dependent of the flow solution and cannot be exactly evaluated in advance. The complex nature of cell-point-face addressing, where the connections does not follow any pattern, is disadvantageous for implementation of spatial discretization schemes. Therefore most solvers including those employed by author achieve lower order of accuracy in space than on structured grids. Due to this and a large bandwidth of linear coefficient matrices generally causes slower convergence on unstructured meshes.

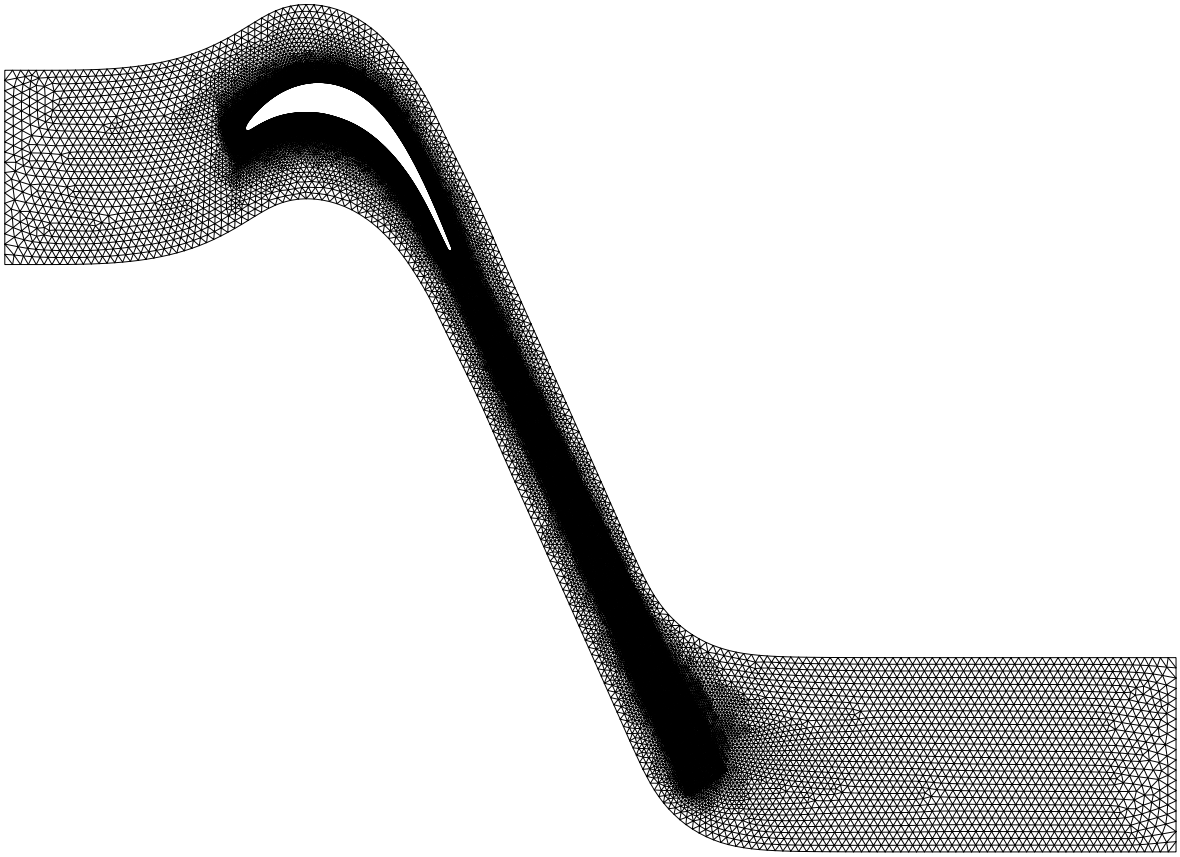

Figure 4: 2D unstructured mesh

4.3 Structured hexahedral mesh

It was later discovered, that the triangle based mesh does not comply with $y_w^+ \leq 1$. Decision was made to try a different approach to structured grid design in order to take advantage of higher order schemes, which the solvers used were capable to apply on such grid.

The former domain was utilized at first, but due to preserving problems with skewed cells a new domain was created manually, inspired by [1], where an identical cascade is analyzed.

The biggest challenge was to keep skewness low when satisfying a strong constraint of pitchwise periodicity. The manual shape features no curvature of this boundary in the front part and its region of prolongation behind the trailing edge is shorter as like as the whole outlet part. The boundaries comprises mainly of straight lines, except for the parabola in the aft part of interblade channel. It is tangential to both lines it meets on its ends and the

shape roughly follows the aft part of the blade camber line. For O-grid topology around the blade surfaces, a curve exactly equidistant to blade at distance $0.1\,[-]$ was computed to determine interface of the fine wall adjacent blocks with surrounding grid. The sets of points generated by MATLAB script were output in a formated point data file and loaded to ICEM CFD. The results of these operations are visible in chapter 4.3, along with the blocking described in upcoming paragraph.

The blocking introduced is double shifted so two more blocks and accordingly more cell columns sit on the suction side surface than on the pressure side, the periodic constraints are pictured by node counts along the boundary edges in chapter 4.3. Both shifts are located in the back of the domain. The initial spacing ($0.0004\,[-]$) and expansion ratio ($1.05\,[-]$) rules are prescribed for all wall normal block edges. The equidistant supply curve ensures the uniform arrangement of boundary layer resolving grid.

All of the wall-tangential node spacings inside the blocks were kept uniform, unless a contraction was needed to accomplish correct expansion ratio on the connection to neighboring block e.g. the trailing edge block. The block covering the leading edge asked for a more delicate treatment, as it is of the "J" shape rather than simple "C", typical for completing the O-grid shape. The point distribution function is set by a manually shaped curve reaching its peak value at the leading edge, allowing the rows of the inlet section cell edges to connect to the LE block with moderate angles and curvature. A detail of the blade surrounding grid is viewed in chapter 4.3

No special refinement is applied in the wake region, since the primitive and stiff constraints characterizing a structured grid are yielding a sufficiently fine resolution in the wake. This region is coarser than in the unstructured grid, but it is not yet sensitive of the exit angle.

Summary of parameters of the two pictured meshes can be found in table 1.

Table 1: Structured and unstructured mesh parameters

Parameter	z-resolution	Unstructured	Structured
2D number of cells		102,216	78,840
Cell type		prisms	hexahedra
Wall faces in 1 layer		1,696	580
ΔY_w		1.5×10^{-3}	0.4×10^{-3}
Domain length	fine / coarse	2 / 0.25	2 / 0.25
Number of spanwise layers	fine	256	384
Number of spanwise layers	coarse	8	16
ΔZ_w	fine	7.8125×10^{-3}	5.2083×10^{-3}
ΔZ_w	coarse	31.25×10^{-3}	15.625×10^{-3}
3D number of cells	fine	26,167,296	30,274,560

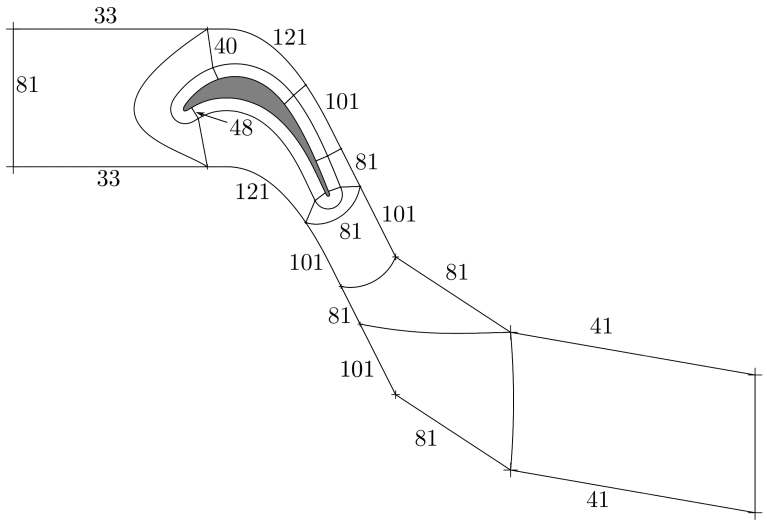

Figure 5: View of the structured domain boundary and grid blocks with edge node counts clarifying the pitchwise periodicity

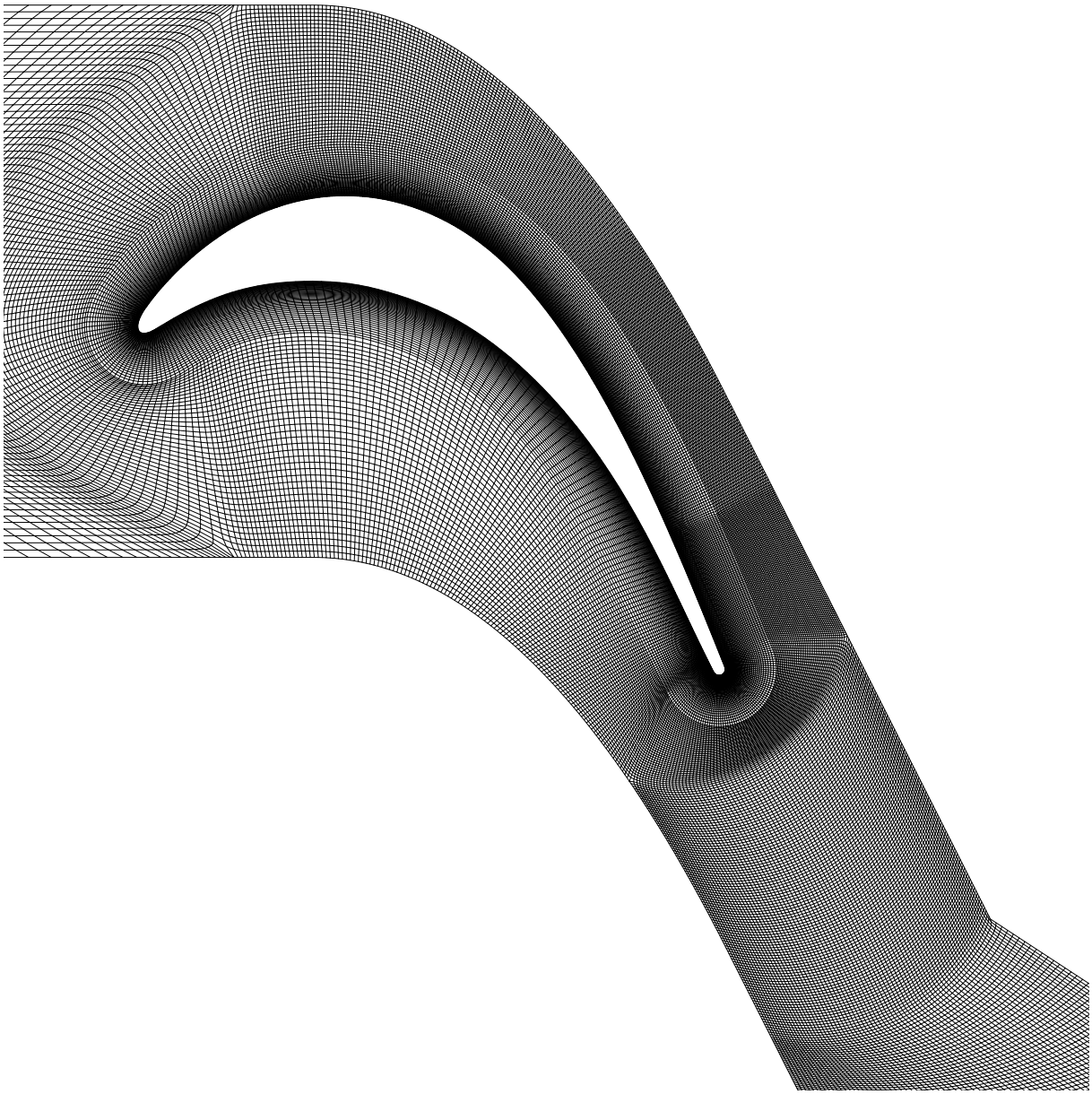

Figure 6: 2D structured mesh

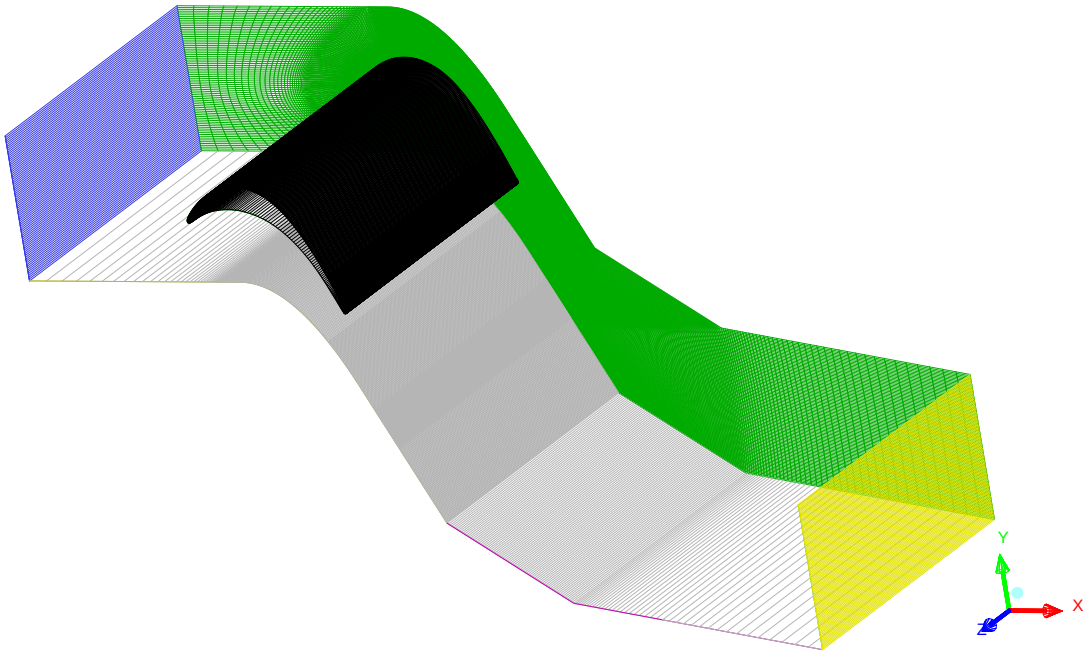

Figure 7: Illustration of structurally meshed domain of $S = 2\,C$

5 Preliminary computations

A lot of minor runs were submitted to validate many aspects of simulation setup. Usually the efforts were to use few computational time and resources and solve particular problems on the fly by interrupting the simulation or editing its data during runtime. This chapter is rather a summary of problems solved than a description of the runs itself.

After the mesh generation, it was first ensured, that the mesh data are correct to read in the native software of ICEM export - FLUENT. FLUENT itself does not recognize periodic boundary conditions set up by ICEM, but the other aspects of mesh were proven to be right.

5.1 OpenFOAM specific setup

This section briefly describes the work flow leading to a desired computation within the mentioned framework with all features needed to attain data of interest. The picking and setting up of the numerical methods from available libraries as well as the data sampling functions being the key points of these actions.

5.1.1 Mesh operations

A fluentMeshToFoam utility of OpenFOAM was used to convert the mesh into OpenFOAM polyMesh directory file structure. The default parameter writePrecision (meaning number of significant digits of "float" data type) defaulting in value of 6 is not sufficient to keep the periodic boundaries aligned. It was changed to 12 for every mesh operation in the process of case setup and was switched back to 6. This was done in favor of avoiding significantly increasing the amount of data generated by simulation, since OpenFOAM applies the writePrecision value to every variable except time.

To prescribe the boundary conditions, it is necessary to run a createPatch utility with underlying dictionary file present in order to link the cyclic boundaries. For parallel runs, a decomposition of the computational domain has to be made.

The decomposePar utility takes care of this. The universal and automatic decomposition method "scotch" was used for all cases exclusively while it is fully automatic and does not have any major drawbacks against any of other methods usually requiring laborious setup. The purpose of this step is to divide the domain into a number of subdomains, each being

treated by single *CPU (central processing unit)* core. The speed of parallel computation directly depends on the quality of decomposition.

In the simplistic terms, all of the processors have to wait for the one which takes the most time to complete one operation, after which a communication between the processors has to be done. These facts yields the basic demands on the decomposition - approximately uniform number of cells for every subdomain, lowest possible number of processor interface patches overall and per each processor, lowest possible number of mesh faces in every processor interface. Obviously this task has multiple solutions which are not easily defined, so an automated algorithm already implemented in the solver is the way to go even with geometry of relatively low complexity. Not only the mesh is split, also the initial field values are propagated.

The last mesh operation before lowering the precision of data outputs is renumbering. As Coudou in [6] has mentioned, reducing the bandwidth and profile of matrices describing the mesh, which are treated by linear solver in each iteration, has a large impact on the total CPU time needed. The default OpenFOAM implementation of Cuthill-McKee method was used always. The ratio of bandwidths before and after renumbering is large especially for smaller grids eg. the 2D meshes for RANS simulations.

5.1.2 Numerical schemes and solvers for LES

The numerical computations in fluid dynamics and some other fields comprise of space and time discretization of fields of resolved quantities by numerical schemes and a solution of created set of linear equations in matrix form.

Since the LES simulations are transient and intended to be time-resolved, the *PISO algorithm (Pressure Implicit with Split Operator)* is used, which predicts the velocity field, computes the pressure field based on velocity prediction and corrects the velocity field according to gained pressure field. Only one loop of this type is imposed in each time-step.

Although not only the PISO algorithm but also the second order implicit time discretization scheme (codenamed backward) are stable for higher time-steps, low Courant number has to be imposed by means of paragraph 2.2.1.2. For near perfect time resolution at $Co \cong 0.25\,[-]$, the OpenFOAM simulations were proven to not be realizable with a reasonable amount of computational resources. $Co = 0.9\,[-]$ is set instead, which is probably the maximum for accurate results with the turbulence effects being dumped sufficiently low.

For convenience, the pimpleFoam solver is used because of its capabilities of adjusting time-step according to prescribed Co (unlike the suggestively named pisoFoam). This may

be inconvenient, for post-processing while time-step is constantly changing, but it is almost inevitable to initialize the simulation. The first time-steps are around 100 times shorter than the stabilized values reached in fully developed flow.

Mainly centered schemes reaching first to second order of accuracy dependent of unstructured or structured mesh respectively are employed for spatial discretization of flow variables. *GAMG (Generalized geometric-algebraic multi-grid)* linear solver is used for pressure equations, residual smoother is employed to solve velocity components.

A command to perform LES simulation with WALE sub-grid scale model is invoked by values in the dictionary turbulenceProperties, the coefficients of the model are kept in default values validated for general use.

5.1.3 Numerical schemes and solvers for RANS

The steady simulation using RANS model of turbulence with SST-kω transport equations were submitted under similar conditions as the LES. The main difference being the simpleFoam solver using *Semi-Implicit Method for Pressure Linked Equations* as a superior choice for steady incompressible simulations and the psoudo-time discretization scheme. This scheme does not evaluate the time derivatives at all. Unlike the unsteady time-stepping, SIMPLE check the convergence in every pseudo-time-step only for reaching a relative decrease in residual values, marching towards more accurate solution.

The spatial discretization was kept the same as for LES. Since the domain is two-dimensional for RANS, boundary conditions at spanwise normal patches of a one layer computational grid are set to empty. This is a general technique how to setup a 2D case in OpenFOAM.

5.2 YALES2 specific setup

Since the aims remain the same, the setup is similar to the one described in chapter 5.1, especially chapter 5.1.2. Besides OpenFOAM being an open source library with literary endless options of customization, there is not so many manual operations involved in setting up commercial solver YALES2. It is designed primarily for solving of two-phase combustion on massive complex meshes, as the official webpage [5] states.

The LES used the incompressible solver and WALE SGS model. The time discretization

was done by fourth order Runge-Kutta method with the identical dynamic global time-step condition defined by $Co = 0.9\,[-]$. Space discretization is second order accurate on an unstructured mesh and fourth order accurate on a structured mesh with schemes used by YALES2.

As stated in paragraph 3.4.2.1, a transient inlet boundary condition prescribing the inlet velocity turbulence explicitly was set. During examination of debugging runs, it was discovered, that the inlet far field is probably too distant from the region of interest and most of the turbulence decays before reaching the blade. However, some notable differences in results were present and are discussed in chapter 7.

Along with the advanced linear solver using *DPCG (Deflated Preconditioned conjugate gradient)* technique, the simulation is quite more time efficient compared to OpenFOAM.

5.3 Runtime data sampling

Although there was still sometime a solver specific approach, the sampled datasets are intended to be identical, another level of document structure therefore is not added here.

The type and amount of the sampling data depends of what is decided to be evaluated. The sampling geometrical locations were prescribed analytically by MATLAB/Octave scripts and the data obtained were thoroughly tested. Some of the locations were changed in a number of preliminary runs or were they kept redundant.

This had to be done carefully because a crucial influence on the simulation runtime by the input/output actions intensity was ascertained. It was experienced, that in massively parallel runs, a residual oscillation occurs at specific data operation cycles, which were therefore disabled. One of the few debugging runs on large meshes was stuck in the initialization process with an automatically assigned time-step reaching unacceptably low values due to this issue.

5.3.1 Blade surface points

For calculating of the pressure and friction coefficients, 256 points along both surfaces of the blade are prescribed. It may be tedious to sample data right on the wall or even prescribe the points precisely enough not to penetrate the boundary. A uniform offset of magnitude lower than the first wall layer cell thickness is created to prevent this issue. The

points were only located in one spanwise normal plane. Although there are suggestions to average the analyzed values along span in 3D transient prismatic cascade cases, the results are mostly in good condition to be presented undoubtedly, at least concerning the influence of this single aspect.

OpenFOAM is equipped by a sampling interpolation scheme internally called cellPointFace and sampling type patchCloud, which comes handy to obtain values of variables right on the boundary faces. The procedure of finding the nearest projection of point to the boundary patch may seem complex, but as far as authors knowledge reaches, there is no other way to get such structured and well controlled set of boundary faces data.

In YALES, the approach is more of a brute force, the offset of points sampled along blade surfaces remains finite. This not a problem for the pressure values, but the values of velocity gradient or friction velocity, which were sampled to calculate the friction coefficient remained of insufficient quality. Due to strictly closed code of YALES2, the type of interpolation is not clear.

5.3.2 Pitchwise lines

Another points inside the domain were needed for both evaluating of already mentioned c_f and c_p and also the pitchwise dependent values of total pressure loss coefficient Y_p and the flow exit angle $\alpha'2$. The location finally used for evaluating the latter two was 25% of C behind the trailing edge, where the rapid gradients are already flattened enough to gain smooth time averaged curves, mostly without physical, but unexpected phenomenons like locally negative Y_p in transient simulations. 128 points per line were prescribed to have a fine resolution of the curves. It may be close to the number of grid cells which the lines pass through.

In order to evaluate the c_f and c_p, where only pitch averaged values are used, the tightest possible line behind the trailing edge is the choice. Here the expected values of mean pressure close to values the very end of the blade surface are observed, for example.

The transient inlet boundary condition of YALES2 LES case requires special treatment for inlet pressure probe. For other simulation it would be sufficient to take the pressure at the inlet patch, which is easily accessible by solver utilities. Despite that, consistency is held and all the inlet pressure data in all the simulations were read over a pitchwise line 10% of C in front of leading edge.

Because both surface points and pitchwise lines are sampled to evaluate identical quantities,

they are dumped at the same time-step, every 10 iterations.

5.3.3 Velocity profile lines and aft suction surface plane

Lower time resolution results are probed over locations clear from figures of the actual data plots in the chapter 7. They are written out every 100th time-step. The 26 velocity profile lines consisting of 128 points each are defined. The description of geometry relates to figures 14 to 16.

The geometry of the plane located in the aft part of the suction surface, where boundary layer turbulent transition or separation is expected, consists of 64 lines perpendicular to the surface. Every line contains 32 locations to be sampled. This definition allow the plane to be curved along the surface and it is the refinement of the former definition by four corner points, while the size of the set was kept. The description of geometry relates to figures 17 to 19.

6 Production runs

Out of all the simulations underwent, three of these are used to reproduce the results presented in chapter 7, They are listed and described in table 2.

An explanation of the term "convective time" has to be given. As the name pronounces, it is the time in the simulations' dimensionless form, which the takes the fluid particle to pass around the blade from leading edge to trailing edge. Since $C = 1\,[-]$ and $u_1 = 1\,[-]$, convective time is approximated to be $t = u/C = 1[-]$.

Table 2: Production runs summary

Simulation run	OpenFOAM RANS	OpenFOAM LES	YALE2 LES
Mesh Type	2D structured	3D structured	3D unstructured
Cluster	Vega	Zenobe	Zenobe
Convective times	-	18.5	24.6
No. time-steps	12500	48620	41370
Wall time $[h]$	0.33	$24 + 5.5$	24
No. of processors	8	1008	1008
Total CPU time h	2.66	$24,16 + 5,51$	24,16
Data produced [GB]	≈ 1	≈ 100	≈ 90

6.1 OpenFOAM RANS

As it is clear from the comparison, the RANS simulation is a regular task which could have simply been performed on a personal computer. Not only the low required computational power makes it easy to be done. Only the last, well converged pseudo-time-step solution is examined. The residuals fell below $1e^{-}7$ and decreased further by a slow rate until the simulation was stopped.

The parallel decomposition was decoded backwards in no time, without excessive amounts of disk space required. Since no time resolving statistics are performed, the sampling of data can be simply rerun on the complete data stored on the 2D mesh containing $\approx 80'000$ elements.

The platform used for the latter mentioned simulation was a Vega cluster operated by *ULB - Université Libre de Bruxelles*. This computer was widely used for debugging as it is not

such occupied as the Tier-1 facility, but still offers 2752 cores at 2.1 GHz. Thanks to the fact that it has large nodes with 64 CPUs and respective amount of RAM per such node, it is capable of some memory-intensive operations that cannot be performed on Zenobe. Those involving the essential mesh decomposition process for LES, which OpenFOAM is not able to run in parallel.

6.2 LES runs

Unlike the previous, many limitations come in practice when running time resolved 3D case on several millions of cells. Post-processing data are attained during runtime and 3D data are never stored due to both large transient input/output loads and static storage space occupation.

Both LES runs have reserved 42 of the 24 core, single processor compute nodes of the Tier 1 supercomputer Zenobe, which is owned and operated by Cenaero research center. By this time, it is equipped with total count of 5760 Intel processors of generation Haswell clocked at 2.5 GHz and 7776 cores of IvyBridge Intel processors at 2.7 GHz. Because of the non-symmetry of the configuration, the access to the its power is divided logically by scheduler software. Because the faster CPUs are assigned to a scheduler queue that allows at most 24 h of wall time and it is recommended by the CÉCI consortium to use this queue, the OpenFOAM LES run had to be relaunched after exceeding this threshold without reaching sufficient amount of resolved time-steps to average valuable results.

6.2.1 YALES run

It is obvious from the table 2, that YALES2 exhibits performance superior to OpenFOAM. For the sake of responsibility for the used resources and the expenses needed to be covered by fundings, it was decided not to relaunch the YALES2 simulation on a later designed structured mesh, even though the data sampling of the first run had some bugs (see chapter 5.3.1). Due to that, direct correlation of performance parameters is impossible. It is rather an assumption based on rigorous facts reviewed in chapter 5.2 that YALES2 would perform even more efficiently on a larger, but structured mesh.

Since YALES2 has computed such large amount of convective time, the time averaging of the data can be made in a safe way. By assumption from figure 8, the time averaging was started at $t = 12$. It may be possible to start earlier, but it is not necessary. The time

averaging period is long enough and all of its contents is statistically converged.

It has to be stated that the values of dimensionless distance reached at the front part of suction side and aft part of pressure side is of value $y_w^+ \cong 2.5$. This means a certain under-resolution of those regions, nevertheless it is believed that such inaccuracies do not have a significant parasitic effect on the turbulent structures development in decelerated flow on the aft suction side.

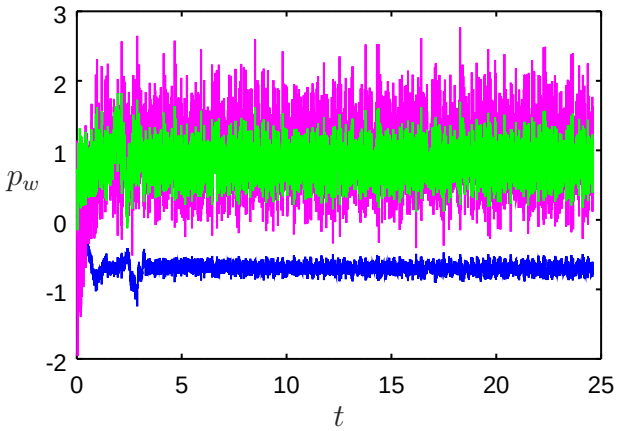

Figure 8: Raw pressure time evolution at arbitrary points on blade surface. Trailing edge (magenta), aft suction side (blue), aft pressure side (green)

6.2.2 OpenFOAM run

Although OpenFOAM was not able to run feasibly on an unstructured mesh, after applying the structured one, it took advantage of higher order spatial accuracy and simplified directives of data output introduced by author and finished the computation. Still, the amount of simulated time is not ideal.

It is not possible to determine whether the time averaging is made right, although the lift and drag coefficient plotted in figure 9, which are very sensitive parameters, have at least converged to a time mean value. Still the amplitude and period of oscillations appears to change in the last part of viewed spectrum. To obtain sufficiently long time span for averaging, it was started at $t = 7$ to average at least 10 flow passing periods.

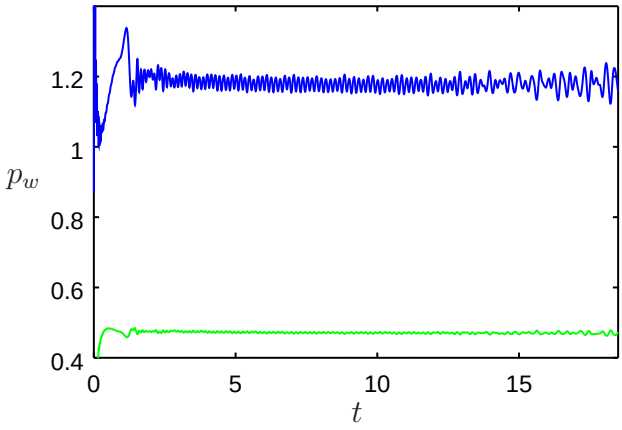

Figure 9: Integral parameters used to estimate statistical convergence in OpenFOAM LES. Lift coefficient (blue), drag coefficient (green)

7 Result analysis

First, a comprehensive comparison of parameters obtained from different simulations along with the reference data is made.

The pressure coefficient pictured in figure 10 is in very close agreement for all datasets along the whole pressure side. The flow here is bounded and the boundary layer is thin due to high and increasing velocity, which is typical for these flow regions of turbine cascade. The front pressure side features a point where computational values reaches zero. This is the point of inlet flow alignment where $p_1 = p_w$ It is missed by the measurement because of its spatial resolution and limited options to reach the surface itself.

The front part of the suction side presents static pressure drop by velocity increase. This happens right behind the stagnation point, which is translated slightly off the leading edge, in the direction of decreasing pressure, as expected. In the graph, it is represented by the first local peak, which is of different value, but very similar position for all suction side curves. Another peak is reached behind 40% of suction surface length. The adverse pressure gradient affects the rest of the suction surface and wall static pressure decreases. RANS solutions starts to diverge off the other curves presented in the last mentioned part, because the adverse gradient is weak. The reference experimental curve is measured at higher Re, so it presents a separation bubble behind 80% of suction surface, which is not present in the computations. Another specific feature of measurement data is the trailing edge value close to 1. This is not reached within computations because of the correctly and uniformly distributed points at the trailing edge, where the measurement was not

performed. The value higher than 1 and the shape of curves indicates the translation of real exit point towards suction side. The green curves, for clarity of the figure mostly cut off the axes span, address large temporal variation of YALES2 LES results. This is due to the unsteady boundary conditions causing oscillating inlet pressure, which may not be in phase with the vortex shedding behind the blade.

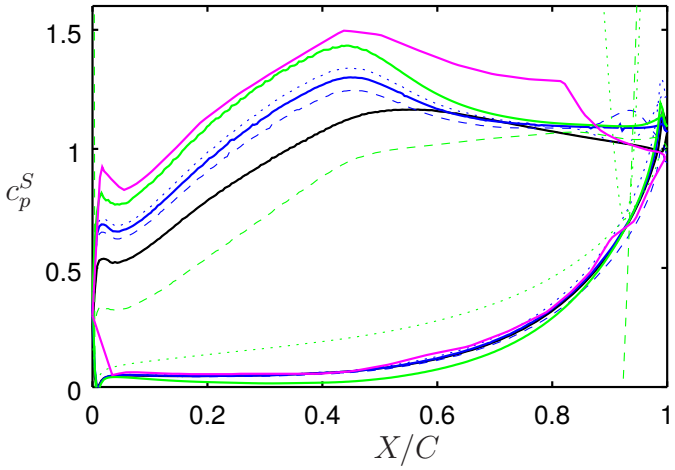

Figure 10: Pressure coefficent: Steiger's measurement (magenta), RANS (black), OpenFOAM LES (blue), YALES2 LES (green). Dotted and dashed styles indicate the the maximum and minimum integral value over blade surface of a single time step in respective transient simulation. Upper curve relates to suction surface, lower for pressure surface.

Friction coefficient is much more sensitive variable, as the large differences in the graph in figure 11 show. The values obtained from YALES2 simulation are not pictured due to sampling issue. The OpenFOAM LES values are much higher than DNS results of the reference article (again obtained for higher Re), the shape is retained and it features negative values, which indicate recirculation of flow along the suction surface. This point is even closer to the tip of the blade thanks to weaker turbulence effects on boundary layer stability in low Re flow.

RANS computations fails to predict the recirculation overall and largely overpredicts the value of friction coefficient. Even the SST $k-\omega$ suited to capture low turbulence cases is not successful here. The rest of the results, namely figures 12 to 14 and 17, confirm this conclusion.

The figure 12 express the mass averaged flow exit angle, both LES runs agree to each other, especially the integral value indicating the deviation angle $\delta \cong 1.5°$. Note that the sampling line is shifted due to the different shape of the domain of structured and unstructured mesh.

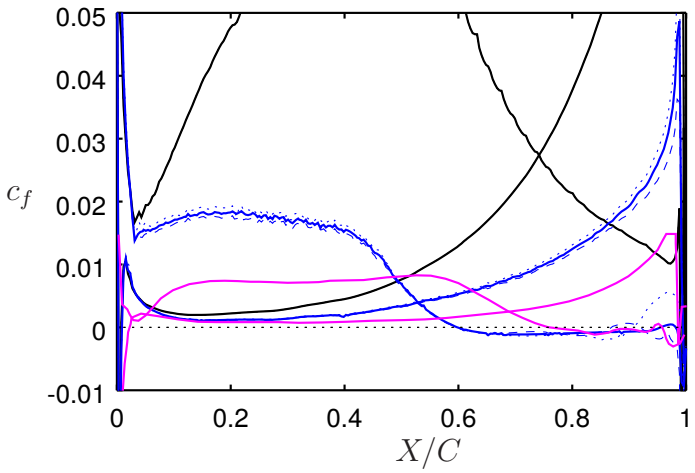

Figure 11: Friction coefficient: 4$^{\text{th}}$ order method simulation taken from [1] (magenta), RANS (solid black), time averaged OpenFOAM LES (blue). Dotted and dashed blue indicate the curves with maximum and minimum integral value over blade surface of a single time-step in LES. Pressure side curves are those peaking near the trailing edge.

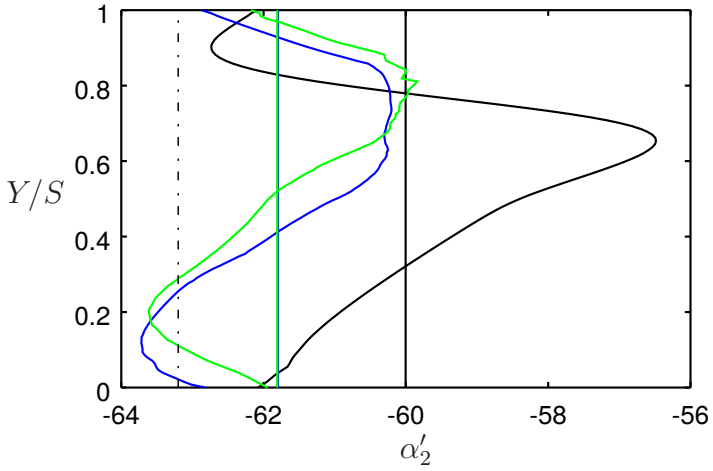

Figure 12: Flow exit angle: RANS (black), time averaged OpenFOAM LES (blue), time averaged YALES2 LES (green). Straight lines indicate mass average. Dash-dotted line for design exit angle.

In the figure 13 see the failure of RANS by overpredicting losses again. The agreement of LES runs is slightly lower regarding the pressure fields than in velocity-based evaluation in figure 12. Slightly negative local values, mostly OpenFOAM-specific are addressed to early start of averaging period, although they are not unphysical.

The probably incorrect picture of velocity field computed by RANS (figure 14 features a very thick boundary layer which is also separated (inflexion points are present in the viewed velocity profiles), but does not undergo turbulent transition nor creates recirculation zone

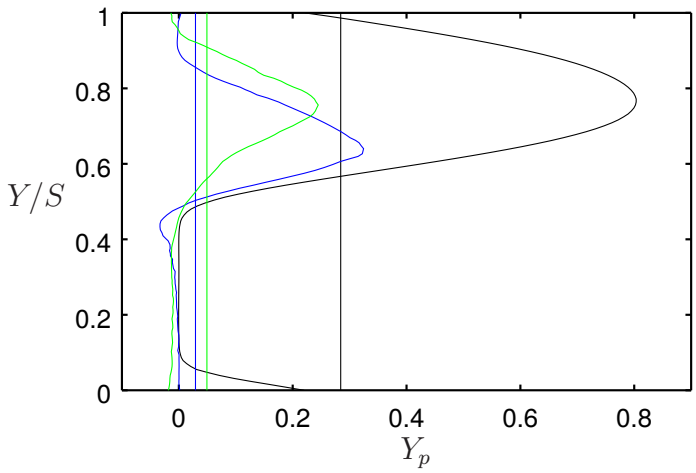

Figure 13: Wake loss coefficient: RANS (black), time averaged OpenFOAM LES (blue), time averaged YALES2 LES (green). Straight lines indicate average value over pitch.

or enclosed separation bubble.

The velocity vector plot in figure 15 confirms predictions of boundary layer separation including region of recirculation from the trailing edge along the suction side. The boundary layer turbulizes while recirculation occurs, however, the intensity of fluctuations and the length of the solid surface is not large enough for the BL to reattach, so the enclosed separation bubble does not occur.

The snapshot of instantaneous velocity profiles in figure 16 gives an idea of how large are the fluctuations. Along with author's sight of the complete data, which are not reproducible here, the most fluctuating region by means of turbulent intensity and frequency of oscillations is the trailing edge, to no surprise.

The vorticity contour plots in figures 17 to 19 gives the detailed information about the region of interest - the aft part of suction side. As already known, there is no negative vorticity in RANS in the viewed region, the flow does not recirculate. Despite that, figures of LES results show clearly that the recirculation reaches to 60% of C. The comparison of mean and instantaneous state may advise that the recirculation region is relatively stable and most of the unsteady features stay in the trailing edge region.

The last figure 20 may advocate the use of such spanwise-long domain since the avalanche-like separation of the captured sturucture would not occur in a narrow periodic domain.

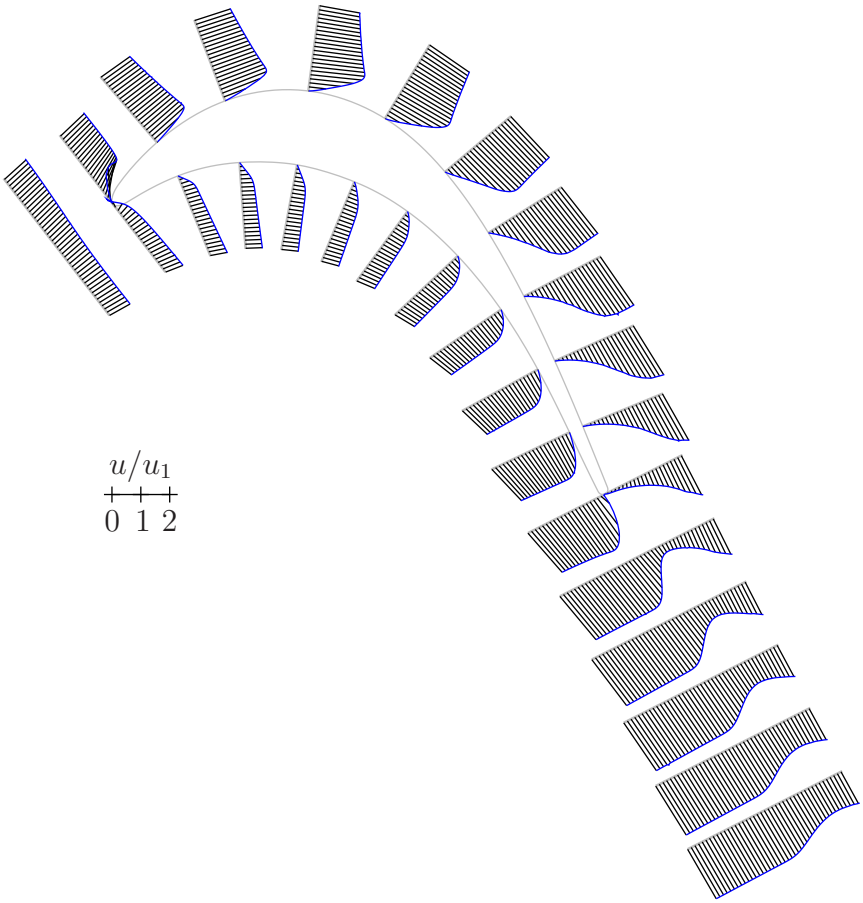

Figure 14: Velocity profiles along blade computed by RANS.

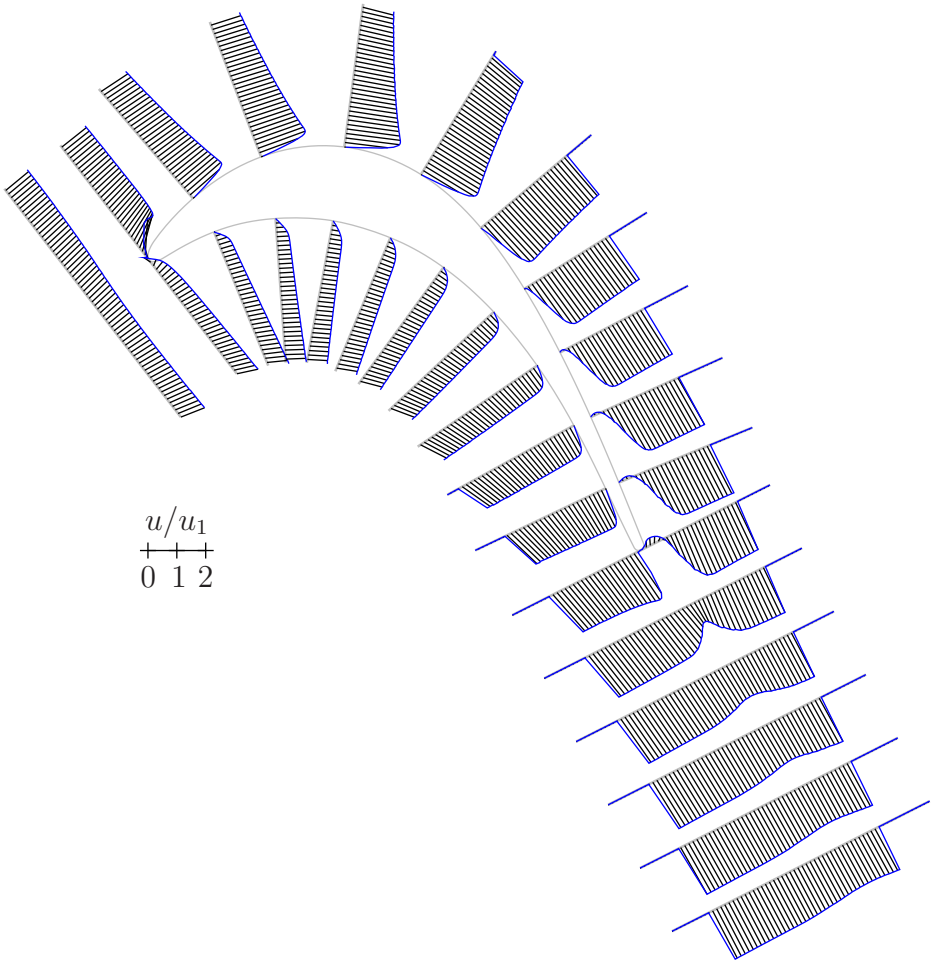

Figure 15: Velocity profiles along blade, time averaged YALES2 LES from $t = 12$.

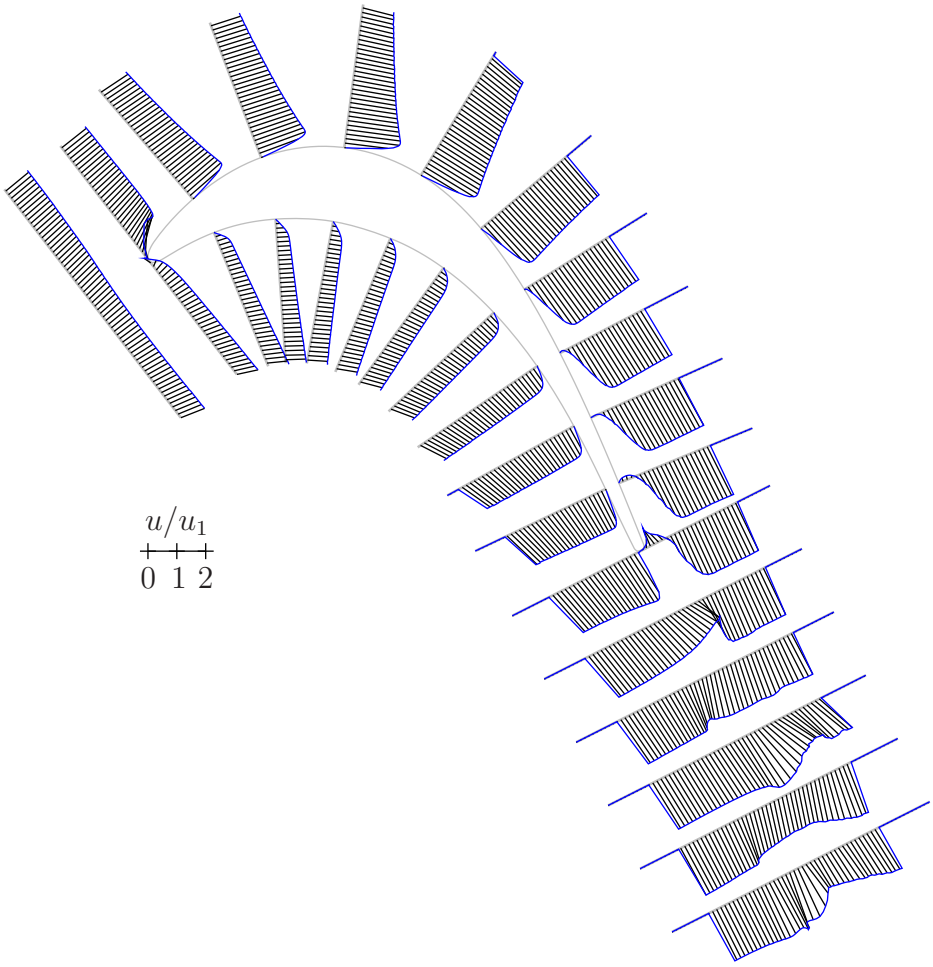

Figure 16: Instantaneous velocity profiles along blade at $t = 15$

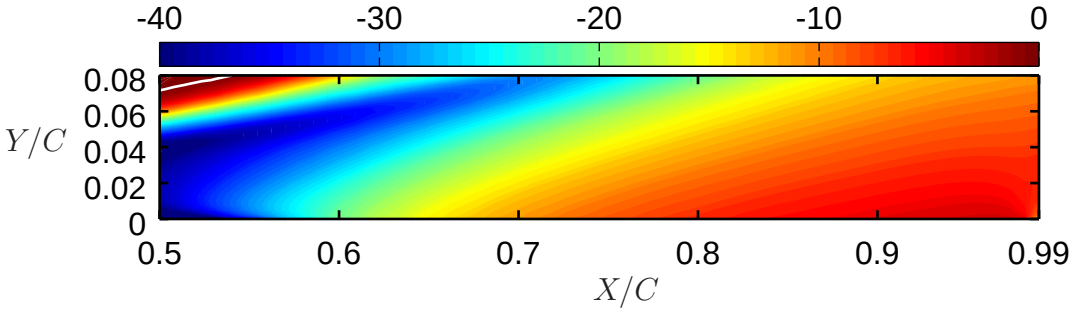

Figure 17: Map of spanwise vorticity at the aft part of suction surface, RANS computation.

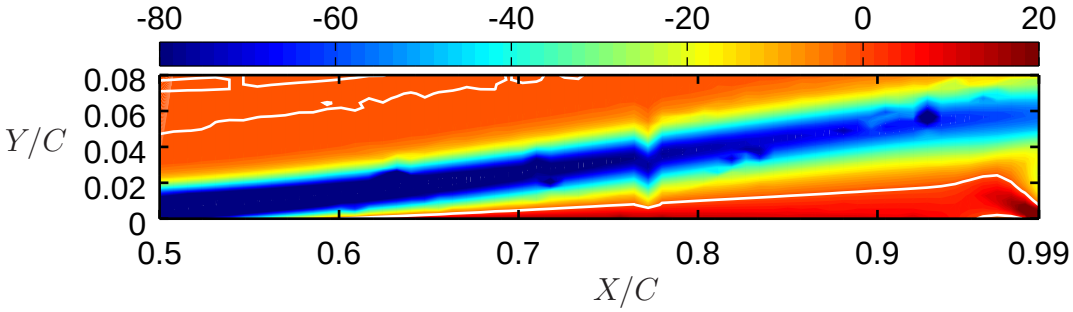

Figure 18: Map of time mean spanwise vorticity at the aft part of suction surface, OpenFOAM LES computation. White contour indicates zero value.

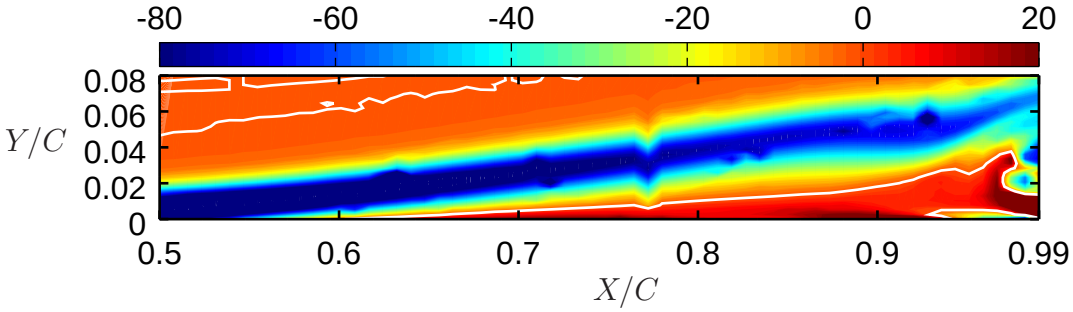

Figure 19: Map of instantaneous spanwise vorticity at the aft part of suction surface, OpenFOAM LES computation at $t = 17.28$. White contour indicates zero value.

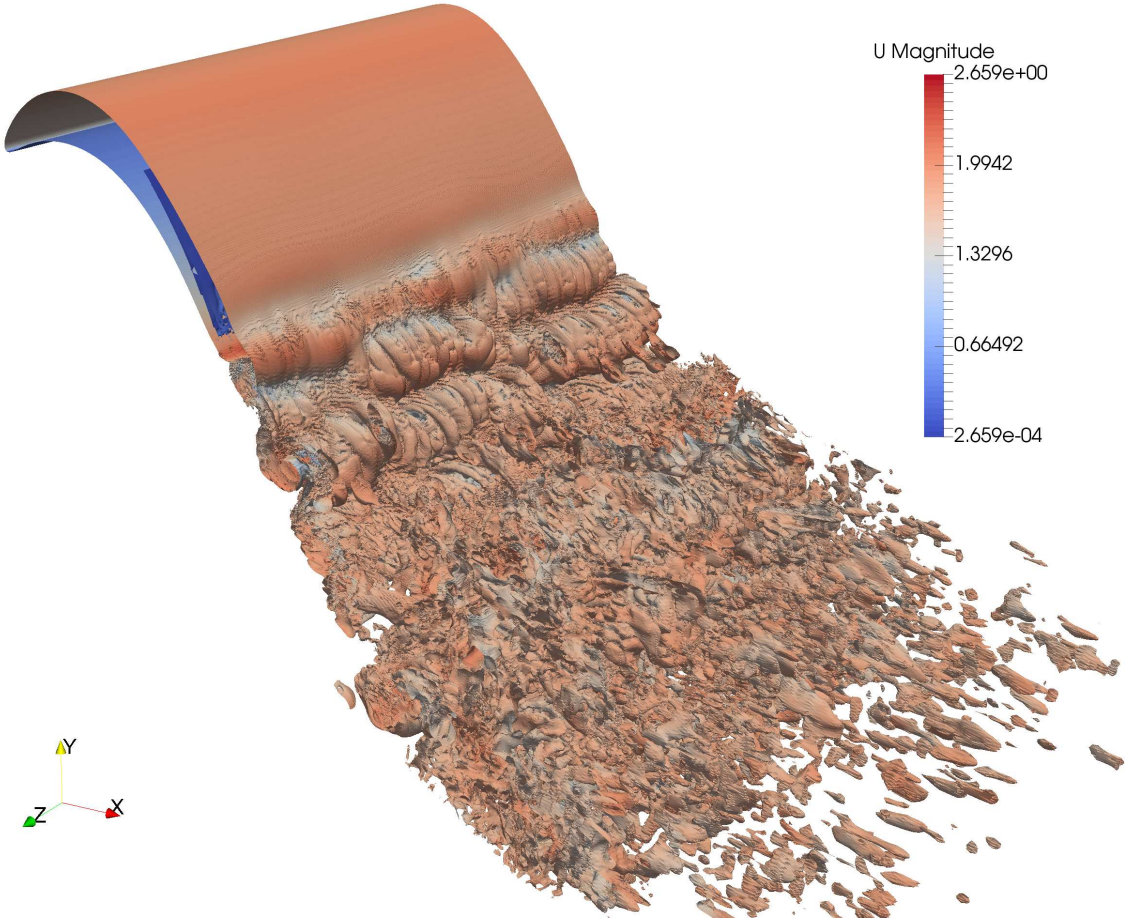

Figure 20: Surface of constant vorticity magnitude of 10. OpenFOAM data snapshot at $t = 17.28$.

8 Writing report

The *Large Eddy Simulation* computational approach of turbine cascade was analyzed. The background theory was revisited in terms of the cascade test theory and practical knowledge. The mathematical basis of the computations is covered too, often by learning from the former source of the invention alone. This is both made mostly from point the view of an engineering student interested in the flow phenomena in turbomachinery.

A well posed problem was constructed from the demands on the results. Two computational grids were designed for checking the capabilities of used solvers. An unstructured mesh was later followed by a structured multiblock mesh of relatively complex 2D topology. A set of boundary conditions was imposed to capture the physical reality at the best possible level. Those including a synthetic turbulence cloud utilized to prescribe realistic velocity inlet. Two dimensional periodicity of the domain was created to separate the flow phenomena and aim to accounting the profile losses as an fundamental part of energy loss in a typical low pressure turbine.

As a main goal, the two solvers designed for massively parallel computing were assessed by extensible comparisons amongst each other and various reference data obtained by by other authors by high fidelity computational and experimental methods of the exact same geometry.

High performance computing facilities including the most powerful Belgian supercomputer were used to finish the simulations on grids of sizes of up to 3×10^7 cells.

Author concludes, that LES, although still unavailable for many, is a superior approach to look into lower turbulent to transitional flows with complex features as like boundary layer separation, high diffusion regions such as that occurred in the studied case. Future work can extend this gained experience and understanding to study higher Re flows possibly employing wall functions to allow not to extend the mesh sizes prohibitively.

It was proven that open source CFD library of OpenFOAM is comparable and competitive alternative to advanced narrow specialized solvers scaling well with proper setup on High Performance Computing machines.

The power of sophisticated algorithms behind the solvers on the edge of scientific and industrial field as like YALES2 were discovered, yet taking the full advantage of them would require a longer immersion into the subject.

The results obtained are satisfactory except the side reference computation by Reynolds Averaged Navier-Stokes equations. The advantages of LES were shown against the full spectrum turbulence modeling. This does not mean a failure in the case analysis, but is rather a conclusion about the limits of the latter CFD techniques. In the presented case a fine line between the capabilities of two presented approaches were drawn, while arguably any better selection than SST $k-\omega$ is possible to study flow of this kind by RANS approach.

References

[1] S. MURMAN A. GARAI, L. DIOSADY and N. MADAVAN. DNS of flow in a low-pressure turbine cascade using discontinuous-galerkin spectral-element method. In *Proceedings of ASME Turbo Expo 2015: Turbine Technical Conference and Exposition*, 2015.

[2] Peter BRADSHAW. *An introduction to turbulence and its measurement*. Pergamon Press, 1st ed. edition, 1971. ISBN 978-1-85617-793-1.

[3] Laurent BRICTEUX. *Simulation of turbulent aircraft wake vortex flows and their impact on the signals returned by a coherent Doppler LIDAR system*. PhD thesis, Universite Catholique de Louvain, 2008.

[4] CARDAMONE, P. *Aerodynamic optimisation of highly loaded turbine cascade blades for heavy duty gas turbine applications*. PhD thesis, University of the German Armed Forces Munich, 2006.

[5] Coria-CFD. YALES2 public page. `https://www.coria-cfd.fr/index.php/YALES2`, 2015.

[6] COUDOU, N. *Numerical and experimental investigations on the aerodynamics of a generic vehicle*. PhD thesis, University of Mons, 2015.

[7] Corentin Carton de WIART. *Towards a discontinuous Galerkin solver for scale - resolving simulations of moderate Reynolds number flows, and application to industrial cases*. PhD thesis, Universite Catholique de Louvain, 2014.

[8] S. L. DIXON and C. A. HALL. *Fluid mechanics and thermodynamics of turbomachinery*. Burlington: Butterworth-Heinemann, 6th ed. edition, 2010. ISBN 978-1-85617-793-1.

[9] Joel H. FERZIGER and Milovan PERIĆ. *Computational methods for fluid dynamics*. Berlin: Springer-Verlag, 3rd rev. ed. edition, 2002. ISBN 3540420746.

[10] KUNTZ M. MENTER F. R. and LANGTRY R. Ten years of industrial experience with the SST turbulence model. *Turbulence, Heat and Mass Transfer*, 4, 2003.

[11] Franck NICOUD and Frédéric DURCOS. Subgrid-scale stress modelling based on the square of the velocity gradient tensor. *Flow, Turbulence and Combustion*, 62 (3), 1999.

[12] BENOCCI C. PIOMELLI U. and van BEECK, J. P. A. J. Large eddy simulation and related techniques: Theory and applications. In *Lecture series*, Rhode Saint Genese, Belgium, 2012. The Von Karman Institute for Fluid Dynamics. ISBN 978-2-87516-028-7.

[13] Hermann SCHLICHTLING. *Boundary-layer theory.* McGraw-Hill, 1979. ISBN 0-07-055334-3.

[14] Rory Douglas STEIGER. *The effects of wakes on separating boundary layers in low pressure turbines.* PhD thesis, Cambridge University Engineering Department, 2002.

[15] Pratt & Whitney. Pw2000 engine. `http://www.pw.utc.com/PW2000_Engine`, 2012.

List of Figures

List of Tables